공학박사 학위논문

# Design of Catalysts for the Oxidative Dehydrogenation of Propane to Propylene and Esterification/ Pyrolysis of 2,3-Butanediol to 1,3-Butadiene

## 프로판의 산화 탈수소화 반응을 통한 프로필렌 제조용 촉매 디자인 및 에스터화/열분해 반응을 통한 2,3-부탄디올로부터 1,3-부타디엔 생산

2015년 2월

서울대학교 대학원

화학생물공학부

백 자 연

# Abstract

## Design of Catalysts for the Oxidative Dehydrogenation of Propane to Propylene and Esterification/Pyrolysis of 2,3-Butanediol to 1,3-Butadiene

Jayeon Baek

School of Chemical and Biological Engineering

The Graduate School

Seoul National University

Olefin and diolefin are unsaturated hydrocarbons which contain more than one carbon-carbon double bond. Ethylene, propylene, and butylene are representative light olefins including diolefins and considered as key building blocks in the chemical industry with the largest production volumes worldwide. These light olefins and diolefins are generally produced from steam cracking of naphtha, however, since the oil crisis has occurred, the necessity of alternative production routes for these light olefins and diolefins through non-oil based processes has driven intensive researches. Currently, the feedstocks are renewed from oil to coal, natural gas, or biomass. It is especially noteworthy that they have brought new perspectives for the effective conversion of alternative feedstocks to promising chemical building blocks in an economical way. The studies referred to herein, contain design of effective catalysts and process demonstration to the desired light olefin and diolefin.

The chromium oxide has been reported to be active catalyst for the oxidative dehydrogenation of propane using $CO_2$ (ODHP). The low surface

area of bulk crystalline chromium oxide and loss of active chromium site, however, limits its use in this reaction. With the goal of preparing a catalyst with an abundance of active sites, highly dispersed chromium oxide on mesoporous silica with different amounts of chromium by a facile sol-gel method were prepared. Catalytic experimental results revealed that the catalyst with a 0.028 Cr/Si molar ratio showed the highest catalytic activity among the catalysts studied. Two types of chromium species, isolated Cr(VI) and polymeric Cr(VI) species, were observed, as evidenced by $H_2$-temperature-programmed reduction. They were designated as 'hard Cr(VI)' and 'soft Cr(VI)' sites, respectively. The initial composition of the soft Cr(VI) in the total Cr(VI) is a major determinant factor in the ODHP performance.

Ni-based catalysts have an excellent ability to activate $CO_2$, even under harsh reaction conditions. The chemisorbed $CO_2$ undergoes a sequential carbon–oxygen bond cleavage to generate CO and activated O ($O^*_{ads}$). Such $O^*_{ads}$ generated on Ni could play a role in the reoxidation of the reduced $CrO_x$ species during the ODHP reaction. The regenerated $CrO_x$ could act as active sites in the ODHP reaction, which leads to reduced deactivation of the catalyst. After the addition of 0.5 wt.% Ni to 10 wt.% Cr/Si (0.5 Ni-Cr/Si), the catalytic activity was stable and the selectivity was high. In addition, *ex situ* XPS results revealed that Cr(III) was maintained only in the Ni-promoted catalyst whereas Cr(III) was easily reduced to Cr(II) in the non-promoted catalyst during the reaction. Consequently, the Ni-promoted Cr/Si catalyst enhances the catalytic stability of propylene in the ODHP reaction.

Finally, a novel strategy is described for the selective production of 1,3-butadiene starting from biomass-derived 2,3-butanediol. Designing desirable catalytic reactions was accomplished by utilizing two hydroxyl functional groups in 2,3-butanediol. One of processes is esterification followed by pyrolysis using glucose fermentation products; 2,3-butanediol, formic acid, and acetic acid. The esterification reaction mixture resulted in diesters and a

highly selective C–O cleavage to 1,3-butadiene over diesters was achieved in the pyrolysis step. The other process is dehydration combined with isomerization of 2,3-butanediol. Through this process, it transforms to 2,3-trans-epoxybutane, 3-butene-2-ol, and 1,3-butadiene, sequentially. The findings reported herein describe an innovative route to high yield of 1,3-butadiene, and is environmentally benign process.

**Keywords:** Cr-MSU-x, chromium state, propylene, oxidative dehydrogenation using $CO_2$, Ni co-catalyst, glucose fermentation products, 2,3-butanediol, esterification and pyrolysis, 1,3-butadiene

**Student Number:** 2009-20997

# Contents

# List of Tables

# List of Figures

# List of Schemes

# Chapter 1. Introduction

## 1.1 Olefins and diolefins for building block of useful chemicals

Light olefins and diolefins which consist of ethylene, propylene, and butylenes are considered as the mainstay of the petrochemical industry. These base chemicals are used as backbone of various types of derivatives ranging from packing materials and synthetic textiles to antifreezing agents, solvents, and coatings [1, 2]. According to a report released in 2010, the worldwide production of olefins as well as diolefins occupies the largest volumes among the produced organic chemicals and summarized in Table 1-1 [3]. Among the light olefins, propylene has the most various derivatives even than ethylene. Propylene is used to produce polypropylene resin (PP), acrylonitrile, acrylic acid, propylene oxide, isopropyl alcohol, and isobutanol through polymerization, ammoxidation, oxidation, hydration, addition of halogen, and oxo reaction. Meanwhile, the shortest diolefin is 1,3-butadiene which is mainly used as raw material for the production of different types of synthetic rubber such as polybutadiene rubber, styrene butadiene rubber, and etc. (Figure 1-1).

**Table 1-1.** Worldwide production of olefins and diolefins in 2010 in thousands of metric tons.

| | U.S.A | Asia[a] | China | Europe |
|---|---|---|---|---|
| ethylene | 23975 | 18237 | 14188 | 19968 |
| propylene | 14085 | 14295 | na[b] | 14758 |
| butadiene | 1580[c] | 2715 | na | 2020 |

[a]Japan, South Korea, and Taiwan. [b]Information not available. [c]1,3-Butadiene rubber grade. Adapted from McCoy *et al* [3].

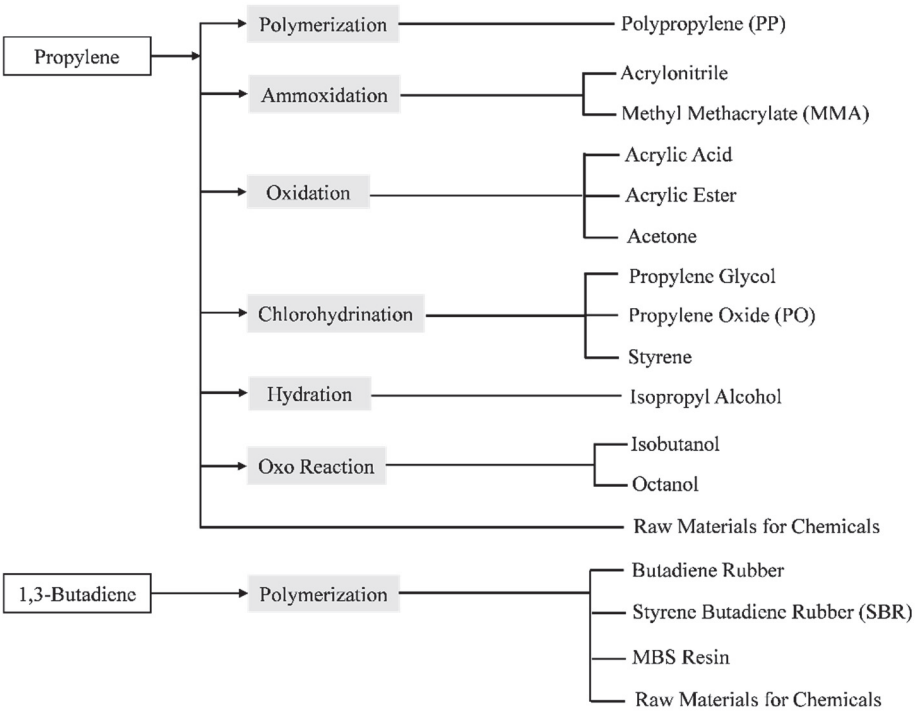


**Figure 1-1.** Propylene and 1,3-butadiene with corresponding derivatives. Adapted from Chiyoda corporation [4].

## 1.2 Production of desired olefin and diolefin

Steam cracking of the naphtha has been the major source of light olefins including diolefins, which is performed in the presence of steam at high temperatures and short residence time [4-8]. To improve energy efficiency, fluid catalytic cracking of naphtha operated at moderate temperature can be another strategy, but two processes are all based on the petrochemistry. With regard to environmental issues, clean energy including biomass or carbon dioxide ($CO_2$) and non-oil energy (natural gas or coal) has been pursued for future raw material (Figure 1-2).

In addition, it is difficult to control composition of products in the case of the current cracking processes, which is obstructive to selective production of desired olefin and diolefin. In the current cracking processes, the yield of propylene and 1,3-butadiene comprises 15% and 5%, respectively [9-12]. To achieve highly selective production of olefin and diolefin, determination of base molecule is considered to be highly important. Propane ($C_3H_8$) is constituents of natural gas and is regarded as base molecule for propylene ($C_3H_6$). Hydrogen molecule ($H_2$) should be subtracted from propane to synthesize propylene which needs dehydrogenation process. The direct dehydrogenation of propane which results in propylene and hydrogen is endothermic reaction ($\Delta_rH^o$=124.31 kJ/mol) and requires high temperature. To reduce reaction temperature, oxygen molecule ($O_2$) are added to extract $H_2$ as water form ($H_2O$). However, added $O_2$ causes over oxidation of hydrocarbons to form carbon dioxide ($CO_2$) and $H_2O$. This over oxidation allows one to

seek to other soft oxidant such as $CO_2$. The oxidative dehydrogenation of propane using $CO_2$ (ODHP) produces $C_3H_6$, carbon monoxide, and $H_2O$ where chemical equilibrium shift occurs by reverse water gas shift reaction. Therefore, the use of $CO_2$ in the oxidative dehydrogenation of propane has beneficial effects with respect to efficient reaction pathway as well as environmental issues. In a similar way, 1,3-butadien which is the smallest diolefin can originate from butylene via dehydrogenation [13-19]. As an alternative and renewable resource, however, 2,3-butanediol that is major product of glucose fermentation liquor can be candidate for the production of 1,3-butadiene. To generate two carbon-carbon double bonds, two hydroxyl groups in 2,3-butanediol should be removed in reaction process. The 1,3-butadiene generation process starting from 2,3-butanediol was not achieved yet, and more exploration is required.

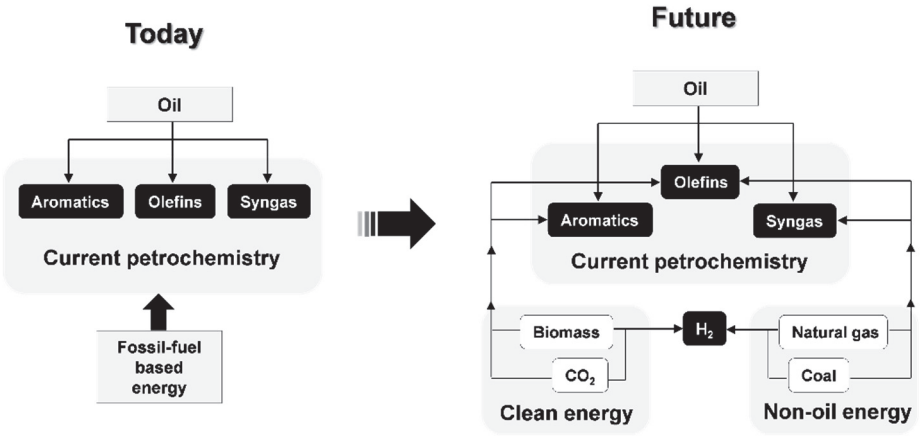


**Figure 1-2.** Diagram of renewed raw materials from current petrochemical chemistry to the clean and non-oil based energy sources. Adapted from Lanzafame *et al* [5].

## 1.3 Design of heterogeneous redox catalysts for propylene

Among the various transition metal oxides, chromium oxide is known to be active for ODHP reaction. As the bulk chromium oxide generally shows low activity by its low surface area, there has been much efforts to develop highly dispersed chromium oxide catalyst supported on mesorporous metal oxides with high surface area. Incipient wetness impregnation method is one of representative catalyst preparation methods and is widely used. However, it is post-synthesis method which requires sequential preparation steps, and is accompanied with limited dispersion of active materials on the supports. The direct incorporation of active materials during synthesis of mesoporous metal oxide can be a solution for the high dispersity.

As a typical mesoporous silica, MSU-x family possess uniform and three-dimensional wormhole-like channels with high surface area and is considered as a promising catalyst support. MSU-x family incorporated with metal oxides are generally synthesized in the neutral pH range where active chromium oxide species can be formed for ODHP reaction. This enables one to design highly active chromium oxide catalyst supported on MSU-x via one-pot synthesis with different amounts of chromium and to investigate the catalytic function of each specific chromium state in the ODHP reaction.

In spite of high activity of chromium oxide catalyst supported on mesoporous silica, it undergoes severe deactivation caused by coke formation and reduction of active chromium site. For the rational design of catalyst to be

stable during ODHP reaction, it is proposed that co-catalyst is added to activate $CO_2$ and regenerate reduced chromium site. The dissociation of $CO_2$ to CO and O is a compulsory step that is taken place in the reverse water-gas shift (RWGS) reaction and nickel (Ni) based catalysts are highly active in this reaction. This phenomenon motivates one to develop tailor-made chromium oxide catalyst supported on mesoporous silica with the addition of Ni as a co-catalyst.

## 1.4 Esterification/pyrolysis for the production of 1,3-butadiene

Over the past several decades, the researches regarding of cracking of naphtha including steam cracking and fluidic catalytic cracking (FCC) process have been carried out. However, with the advent of eco-friendly society, the research on the production of olefin as well as diolefin has moved from petrochemical based resources to renewable raw material. In this respect, biomass can play a leading role as sustainable energy resources with replacing petrochemical based processes. Nevertheless, there was not much advance in the production of 1,3-butadiene from biomass-based resources up to this day.

As one of the simplest monosaccharides found in plants, glucose can be converted into various types of useful chemicals. Through the fermentation process catalyzed by microorganisms, it can produce 2,3-butanediol mainly accompanying many other fermentation byproducts such as formic acid, acetic acid, acetoin, lactic acid, and succinic acid. The catalytic conversion of 2,3-butanediol to 1,3-butadiene was rarely reported and pioneering of novel process development is needed. It is proposed that esterification between 2,3-butanediol and acids produced from glucose fermentation products followed by pyrolysis can selectively yield 1,3-butadiene. In addition, it is also demonstrated that 2,3-butanediol can be converted to 1,3-butadiene through consecutive process of dehydrative epoxidation, isomerization, and acid catalyzed dehydration.

## 1.5 Objectives

This thesis mainly consists of designing catalysts and process for the production of propylene and 1,3-butadiene through understanding redox phenomenon during catalytic reaction.

Following this introduction, in Chapter 2, the synthesis of highly dispersed chromium oxide catalysts with superior redox property supported on mesoporous silica is discussed. The chromium oxide can be divided into two types and it allows one to define active site of chromium for ODHP reaction.

The strategy to reduce deactivation of chromium oxide catalyst supported on mesoporous silica in ODHP reaction is proposed in Chapter 3. Specifically, Ni as co-catalyst plays the role of dissociating $CO_2$ and activated O is used to regenerate reduced chromium site.

Finally, novel process for the production of 1,3-butadiene from biomass-derived 2,3-butanediol is developed and described in Chapter 4. The reaction mechanism is investigated and proper catalyst at each process is suggested.

# Chapter 2. Insight into the Nature of Catalytically Active Chromium Sites via Highly Dispersed Chromium Oxide Catalysts Supported on MSU-x for the Oxidative Dehydrogenation of Propane Using $CO_2$

## 2.1 Introduction

Propylene is one of the most important building blocks in the petrochemical industry for producing polypropylene, propylene oxide, and acrylonitrile [20−22]. The oxidative dehydrogenation of propane (ODHP) reaction is considered an attractive process alternative to steam cracking and FCC [20] for producing propylene. The ODHP reaction represents a route for economically converting low-cost saturated hydrocarbons into value-added olefins [23−26]. The use of oxygen as the oxidant in the ODHP reaction is thermodynamically favorable (an exothermic reaction) but shows low selectivity for propylene due to the fact that oxygen reacts readily with the products [27−30]. Carbon dioxide ($CO_2$) can be a substitute for oxygen, since it serves as a soft oxidant, thus preventing the overoxidation of the products [31−33]. In addition, reducing the levels of $CO_2$ and utilizing it are an urgent subject for realizing a sustainable society [34−36].

A number of transition metal oxide catalysts, such as indium oxide, gallium oxide, vanadium oxide, and chromium oxide, have been reported to be active for the ODHP reaction [21, 37−58]. In particular, chromium oxide has been shown to be highly active for the ODHP reaction in the presence of $CO_2$ [24, 40]. The low surface area of bulk crystalline chromium oxides, however, limits its use in this reaction. With the goal of preparing a catalyst with an abundance of active sites, we prepared a series of samples that contain highly dispersed chromium oxide on mesoporous silica with different amounts of chromium by a facile sol−gel method.

It is generally considered that coordinatively unsaturated Cr(III) in chromium species act as active sites in dehydrogenation reactions [43−45]. Accordingly, several groups have reported that coordinatively unsaturated Cr(III), formed from the reduction of higher-valence states (i.e. Cr(VI)), is an active site in this reaction [46−49]. This claim is supported by the fact that higher-valence chromium states are instantly reduced when they come into contact with alkanes at high temperature [50].

Interestingly, the degree of crystallization of the chromium species is also considered to be another important factor in the dehydrogenation reaction. Kumar et al. [50] reported that isolated chromium species are more active for the dehydrogenation reaction than crystalline α-$Cr_2O_3$ when SBA-15 is used as the support, whereas oligomeric chromium species are more active than isolated chromium species when γ-$Al_2O_3$ is used as the support. However, they were not able to compare the catalytic activity of chromium species (isolated vs oligomers) on SBA-15 because oligomeric chromium species

supported on SBA-15 were not prepared. Consequently, this implies that the synthesis of the polymeric Cr(VI) species on mesoporous silica results in an efficient catalysts for the ODHP reaction and could function as an active center.

MSU-x family, a typical mesoporous silica, has uniform and three-dimensional wormhole-like channels [51] which is favorable for the diffusion of molecules as well as a high surface area and, thus, could be utilized as a promising catalyst support [43]. Here, x is a number or a letter of the used surfactant type. To date, chromium-based mesoporous silica catalysts have been synthesized under highly acidic (Cr-SBA-1, [52] Cr-SBA-15, [53] and Cr-MSU-x [47]) or basic (Cr-MCM-41 [54]) conditions. The types of chromium species formed are, however, strongly dependent on the pH of the aqueous solution used in the synthesis [55]. At pH values lower than 2, chromium species are formed as tri- and tetrachromates (respectively, $Cr_3O_{10}^{2-}$ and $Cr_4O_{13}^{2-}$) which are more highly polymerized and susceptible to forming crystalline α-$Cr_2O_3$. In the pH range of 2−6, smaller chromium anions, such as dichromate ($Cr_2O_7^{2-}$), are formed, which leads to a better dispersion of chromium species on the MSU-x surface.

Above pH 8, only isolated $CrO_4^-$ is stable, but it does not possess a high activity for the ODHP reaction. Therefore, we developed a new method for the synthesis of highly dispersed chromium oxide on a MSU-x support at pH ~ 4 without any additional titration for use as a potentially promising catalyst for ODHP reactions using chromium(III) acetate hydroxide ($(CH_3CO_2)_7Cr_3(OH)_2$). Here, we used a $(N^0M^{n+})I^0$ pathway developed by

Pinnavaia et al. [56] wherein $N^0$ is a nonionic polyethylene oxide surfactant and $I^0$ is an electrically neutral silica precursor. An electrostatic control is introduced into the assembly process through chromium cations ($M^{n+}$). Our strategy involved the use of chromium(III) acetate hydroxide ($(CH_3CO_2)_7Cr_3(OH)_2$), which provides the electrostatic driving force for the ($(N^0M^{n+})I^0$, $M^{n+}$: Cr(III)) pathway and also functions as a precursor for active materials. The steric effect of the ligand in ($(CH_3CO_2)_7Cr_3(OH)_2$) also helps the chromium species to be highly dispersed on the catalyst support, similar to chromium acetyl acetonate ($Cr(acac)_3$) [46].

In the present work, highly dispersed chromium oxide on MSU-x (Cr-MSU-x) with different amounts of chromium was prepared with the goal of creating chromium species in which the activity is dependent on the weight of metal loading [57, 58]. This would enable one to investigate the nature of the chromium species and the catalytic function of each specific chromium state in the ODHP reaction. The correlation between catalytic activity and characterization results obtained from temperature-programmed reduction experiments would permit a better understanding of the nature of the active chromium species for ODHP reaction. We then compared the Cr-MSU-x catalysts with the $CrO_x$/MSU-x catalysts prepared using the conventional incipient wetness impregnation method.

## 2.2 Experimental

### 2.2.1 Preparation of the Cr-MSU-x catalysts

Polyethylene glycol hexadecyl ether (Brij® c10), chromium(III) acetate hydroxide ($(CH_3CO_2)_7Cr_3(OH)_2$), and tetraethyl orthosilicate (TEOS) were purchased from Sigma-Aldrich; and used as the sources of template, chromium, and silicon, respectively. A typical procedure for preparing Cr-MSU-x catalysts is described as follows: A solution of surfactant was prepared by resolving 1.78 g of Brij® c10 in 100 ml of water at 45 $^oC$ under rigorous stirring. A weighed amount of the chromium precursor ($(CH_3CO_2)_7Cr_3(OH)_2$) was then dissolved in the surfactant solution where the Cr/Brij® c10 molar ratio ranged from 0.1 to 2.5. The solution of surfactant and chromium was then stirred at 45 $^oC$ overnight to completely dissolve the acetate form of chromium. After adding 14.5 ml of TEOS to the mixed solution of surfactant and chromium, the resulting solution was stirred at 45 $^oC$ for 24 h. The color of the resulting solutions was initially a pale-green but became dark-green with increasing molar ratio of Cr/Brij® c10. The resulting solutions were then placed in an oven and aged without stirring at 100 $^oC$ for 24 h. The solid products were separated by filtration, washed thoroughly with deionized water and dried at room temperature for 48 h. The final products were obtained after calcination in a stream of air at 650 $^oC$ for 3h to remove the template. Here, we denote the Cr-MSU-xN where N indicates the Cr/Si molar ratio multiplied by $10^3$.

### 2.2.2 Characterization of Cr-MSU-x catalysts

Elemental analyses of the Cr-MSU-x catalysts series were performed by scanning electron microscopy (SEM, Zeiss Supra 55) equipped with an energy-dispersive x-ray spectroscopy (EDS) module with an accelerating voltage of 15 kV. The X-ray diffraction (XRD) patterns were obtained in two ranges of 1-10$^{o}$ and 10-80$^{o}$ using a SAXS with GADDS and Rigaku D-MAX2500-PC powder X-ray diffractometer, respectively with Cu Kα radiation (1.5406 Å). The $N_2$ adsorption-desorption isotherms were recorded on a Micrometrics ASAP-2010 system. The specific surface area of the samples was determined by the BET method. The total pore volume and pore size distributions were calculated from the adsorption branches of the isotherms using BJH methods. High resolution transmission electron micrograph (HR-TEM) images were obtained on a JEOL JEM-3010 microscope with an acceleration voltage of 300 kV. In order to explore the element distribution mapping on the samples, an analytical high-angle annular dark-field scanning transmission electron microscopy (HAADF-STEM, Tecnai F20-FEI, 200 kV) equipped with energy dispersive X-ray spectroscopy (EDS, Tecnai 136-5-EDAX) was used. $^{29}$Si MAS NMR spectra of the samples were recorded on a Bruker Avance II 500 MHz spectrometer operating at a frequency of 99.4 MHz. The magic angle spin speed used for $^{29}$Si spectral recording was 7 kHz. Ultraviolet-visible (UV-Vis) spectra were recorded with a Jasco V670 spectrometer, using diffuse reflectance spectroscopy (DRS) technique. The powdery sample was loaded into a

quartz cell, and spectra were collected at 200-1000 nm referenced to $BaSO_4$. UV-Raman spectroscopic measurements were carried out on a MonoRa750i/ELT1000 spectrometer. The spectra were recorded with a 325 nm excitation laser provided by a He-Cd source. Spectra were recorded at an exposure time of 30s and an accumulation number of 5. Fourier transform infrared attenuated total reflection (FT-IR/ATR) spectra were obtained using a PerkinElmer Spectrum 100 FT-IR. A diamond prism was used as an internal reflecting element for the FT-IR/ATR analysis. The temperature-programmed reduction analysis was performed with a Micrometrics Autochem II chemisorption analyzer using a 10% $H_2$/Ar mixture at a total flow rate 50 $cm^3$ $min^{-1}$. The sample was heated at a rate of 10 $^oC$ $min^{-1}$ to the final temperature of 600 $^oC$. $H_2$ consumption during the TPR experiments was measured by means of a thermal conductivity detector (TCD). The amount of coke deposited on the catalyst was determined by CHNS analysis (CHNS-932, LECO). The over-reduction of the catalyst was carried out in a stream of 10% $H_2$/Ar gas (50 $cm^3$ $min^{-1}$) at 650 $^oC$ for 3h using a Micrometrics Autochem II chemisorption analyzer.

### 2.2.3 Catalytic reactions

The dehydrogenation of propane in the presence of $CO_2$ was carried out in a flow-type quartz reactor packed with 200 mg of catalyst, and the reactor was then placed in an electric furnace. The temperature of the catalyst bed was monitored by a K-type thermocouple controlled by a PID controller. The

catalyst was preheated at 600 $^{o}$C in a stream of dry $N_2$ (30 $cm^3$ $min^{-1}$) for 0.5 h. The dehydrogenation feed consisted of a mixture of $C_3H_8$:$CO_2$:$N_2$=1:1:8 and the total flow rate was 30 $cm^3min^{-1}$. For the controlled experiment, direct dehydrogenation of propane in the absence of $CO_2$ was carried out using $C_3H_8$:$N_2$=1:9 feed. The feed and reaction products were analyzed using an on-line gas chromatograph (Donam DS 6200) equipped with two columns (Porapak Q and molecular sieve) and two detectors (flame ionization detector and thermal conductivity detector). $CO_2$ and C2-C3 hydrocarbons were separated in a column packed with the Porapak Q whereas $N_2$, CO and C1 were separated using a molecular sieve. FID and TCD were used for quantification of C1-C3 hydrocarbons and non-hydrocarbons ($N_2$, CO, and $CO_2$), respectively. The regeneration treatment was carried out under a stream of air (50 $cm^3$ $min^{-1}$) at 650 $^{o}$C for 3 h, followed by an ODHP reaction test. The conversion, selectivity, and yield of propylene were calculated using the following equations:

$$C_3H_8 \text{ conversion } (\%) = \frac{C_3H_{8\,in} - C_3H_{8\,out}}{C_3H_{8\,in}} \times 100$$

$$C_3H_6 \text{ selectivity } (\%) = \frac{nC_3H_6}{nC_3H_6 + (2/3)nC_2H_6 + (2/3)nC_2H_4 + (1/3)nCH_4} \times 100$$

$$C_3H_6 \text{ yield } (\%) = \frac{C_3H_8 \text{ conversion} \times C_3H_6 \text{ selectivity}}{100}$$

where n is a number of moles of hydrocarbons. As the coke formation is instantaneous and time-dependent the conversion of propane into coke was

not considered in the calculations. In addition, the conversion of propane to coke, as measured by CHNS, for the catalyst after a 2 h ODHP reaction was 1.1 wt.%.

## 2.3 Results and discussion

### 2.3.1 Catalyst morphology and pore structure

The Cr and Si elemental contents of the Cr-MSU-xN catalysts are summarized in Table 2-1. As the amount of chromium precursor used in the synthesis process was increased, the Cr/Si molar ratio also increased from 0.003 to 0.082. Figure 2-1 shows XRD patterns of the Cr-MSU-xN catalysts in two different regions of 2θ angles. In the 2θ range of 1-10° a single broad diffraction line is observed at about 2θ = 1.08°, corresponding to $d_{100}$ (8.2 nm) reflections and in agreement with most patterns of MSU-x materials reported by other investigators [47, 67]. Even in the case of the catalyst with the highest chromium loading (Cr-MSU-x82) a single peak at 2θ = 1.08° is still observed, indicating that the mesoporous structure of the materials was maintained. In the 2θ range of 10-80°, only the characteristic peak related to silica is observed up to a Cr/Si molar ratio of 0.051. This means that chromium oxide is highly dispersed on MSU-x, as a result, its size is too small to be detectable. On the other hand, the Cr-MSU-x82 catalyst shows peaks related to crystalline chromium oxide, indicating the formation of α-$Cr_2O_3$.

The $N_2$ adsorption-desorption isotherm and pore size distribution of the pure MSU-x and Cr-MSU-x51 (the largest amount of chromium among the samples without any formations of crystalline chromium oxide) are shown in Figure 2-2. The isotherms of the pure MSU-x and the Cr-MSU-x51 catalyst

are similar to a type IV isotherm and exhibit a H2 type hysteresis loop at relative pressures ranging from 0.4~0.7 except for the fact that the pure MSU-x contains additional textural pores. This indicates that both pure MSU-x and Cr-MSU-x51 catalyst have well-developed mesoporous structures with pore necking in the 3D faulted structure [56]. The pore size, calculated from the BJH adsorption branch, is in the range from 2 to 5 nm for both the pure MSU-x and Cr-MSU-x51 catalysts and their average pore size is about 4.8 and 4.2 nm, respectively. In addition, all the other Cr-MSU-xN catalysts show similar isotherms and pore size distributions indicating that the overall mesoporous structure is well maintained, even when a high amount of chromium is deposited on the MSU-x surface. The surface area and pore volume of the Cr-MSU-xN catalyst series are, however, decrease with increasing in the Cr/Si molar ratio indicating that mesopores in Cr-MSU-xN are covered by chromium oxide when relatively high amounts of chromium are used in the preparation (Table 2-1).

The HR-TEM image (Figure 2-3a) confirms that the Cr-MSU-x51 catalyst contains three dimensional wormhole-like channels. The pore size, as determined from TEM images, is in good agreement with the average pore size from BJH result. In order to examine the dispersion of chromium oxide, an analytical STEM with large angle detection was used for 2-D atomic mapping (Figure 2-3b and c). From this 2-D atomic mapping image we were able to confirm that small clusters of chromium oxide are highly dispersed throughout an entire Cr-MSU-x51 structure without the formation of large bulk state of chromium oxide. This highly dispersed chromium is also

consistent with data for Cr-MSU-x28.

$^{29}$Si MAS NMR spectra of pure MSU-x and Cr-MSU-x28 are shown in Figure 2-4. There are three distinct peaks corresponding to $Q_2$, $Q_3$, and $Q_4$ in both the pure MSU-x and Cr-MSU-x28 materials without no noticeable differences between the two. According to Pinnavaia et al., [59] broadening of the $Q_4$ peak width and the decrease in $Q_2$- and $Q_3$- Si sites along with an increase in $Q_4$ are mainly caused by substitution with an isomorphous transition metal substitution. Maintaining three sites of silica indicates that isomorphous chromium metal substitution has not occurred after the chromium precursor was added.

### 2.3.2 Characterization of the chromium species

The oxidation state and coordination of chromium in Cr-MSU-xN catalysts can critically influence catalytic activity. In order to investigate this, UV-Vis DRS experiments were carried out. All spectra of the Cr-MSU-xN catalysts are given in Figure 2-5. Two intense bands centered at 267 and 373 nm, which are usually assigned to O → Cr(VI) charge-transfers in isolated chromium oxide with a tetrahedral symmetry, appeared as the main absorption bands for all samples listed in Figure 2-4 [47]. These two bands at 267 and 373 nm are assigned to tetrahedral chromate transitions $^1T_2 \leftarrow {}^1A_1$ ($1t_1 \rightarrow 7t_2$ and $6t_2 \rightarrow 2e$) and $^1T_2 \leftarrow {}^1A_1$ ($1t_1 \rightarrow 2e$), respectively. The peak at 483 nm is also assigned to a Cr(VI) transition $^1T_1 \leftarrow {}^1A_1$ ($1t_1 \rightarrow 2e$) [60]. The intensity of this peak increases gradually as the Cr/Si molar ratio is increased

up to 0.051. This band is closely related to the distortion of the Cr(VI) group from a tetrahedral symmetry. The distortion of isolated chromium oxide is reported by Cavani et al. [60] to be related with the degree of oligomerization in the chromium species, i.e., the formation of dimers or polymeric chromium oxide as a consequence of polymerization process. Therefore, the gradual increase in the intensity at 483 nm is caused by the formation of oligomers, which have a lower symmetry than a tetrahedral structure. When the Cr/Si molar ratio increases to 0.082, a new band at 614 nm appears, while the band at 483 nm is slightly decreased. The band at 614 nm corresponds to the typical octahedral symmetry $T_{2g} \leftarrow A_{2g}$ transition in $\alpha$-$Cr_2O_3$ clusters [53, 61]. Thus, the appearance of the peak at 614 nm and the decrease in the intensity of the band at 483 nm is caused by the formation of crystalline chromium oxide. These UV-Vis DRS results are consistent with data obtained in the XRD experiments.

UV-Raman spectra of Cr-MSU-xN catalysts are shown in Figure 2-6. Here, UV-Raman spectroscopy was used to avoid the fluorescence interference from the molecular sieves or related materials [62]. In the presented data, an intense and sharp band at 983 $cm^{-1}$ is observed in the case of the Cr-MSU-xN catalysts, while the band intensity is very low in the Cr-MSU-x3 sample. Wechhuysen et al., [55] reviewed the Raman spectra of a number of supported chromium oxides and concluded that the band at 980-990 $cm^{-1}$ can be assigned to Cr-O stretching of the dehydrated isolated chromate species ($CrO_4^{2-}$), while the band at 1000-1010 $cm^{-1}$ can be ascribed to the Cr-O stretching of dehydrated polymeric chromium oxide.

Unfortunately, overlapping of two bands made it difficult to discriminate polymeric chromium oxide from isolated chromium oxide. As the chromium concentration increases, the band at 983 $cm^{-1}$ decreases indicating that polymeric chromium species are formed during the polymerization process of isolated chromium oxides.

FT-IR spectroscopy is a useful technique for characterizing chromium species in catalysts. Figure 2-7 shows the FT-IR/ATR results for the Cr-MSU-xN catalysts. The high frequency region between 1000 and 1250 $cm^{-1}$ corresponds to silicon-oxygen stretching motions while the band at 796 $cm^{-1}$ is assigned to the vibration of silicon about bridged oxygen [63]. A weak IR band appears at 900 $cm^{-1}$, a much lower value than has been previously assigned in other literature reports to a Cr(VI)-O vibration at about 941 and 950 $cm^{-1}$ in the Cr-SBA-15 and $CrO_x$/SBA-15 samples, respectively [53]. This shift might be caused by differences in the local environments in Cr-MSU-xN catalysts, Cr-SBA-15, and $CrO_x$/SBA-15. Meanwhile, the Cr(VI)-O vibration band increases gradually up to a Cr/Si molar ratio of 0.051, indicating an increase in the polymeric Cr(VI) concentration. In the case of the Cr-MSU-x82 spectrum, the 900 $cm^{-1}$ band has nearly disappeared, while two distinct bands are observed at 558 and 612 $cm^{-1}$ which are characteristic of crystalline $\alpha$-$Cr_2O_3$ [64].

2.3.3 Reducibility of the Cr-MSU-x catalysts

The reducibility of a catalyst plays a key role in dehydrogenation reactions that involve a redox mechanism:

$$C_3H_8 + MeO_x \rightleftharpoons C_3H_6 + MeO_{x-1} + H_2O \quad \cdots\cdots (3\text{-}1)$$

$$CO_2 + MeO_{x-1} \rightleftharpoons CO + MeO_x \quad \cdots\cdots (3\text{-}2)$$

Therefore, the ability to remove hydrogen from propane is related to the reduction of the chromium species in Cr-MSU-x. $H_2$-TPR profiles of the Cr-MSU-xN catalysts are shown in Figure 2-8. The presented peaks are normalized by the weight percent of chromium in the Cr-MSU-xN catalysts. The appearance of reduction peaks can be affected either by the amount of chromium or the interaction between chromium oxide and the support. Two reduction peaks at about 270 and 380 $^oC$ can be seen for all samples and this can be attributed to the reduction of Cr(VI) to Cr(III) and Cr(II) as well [43, 47, 65, 66]. The TPR results combined with the UV-Vis DRS results above clearly show that chromium exists as Cr(VI) state in the samples prepared using Cr/Si molar ratios ranging from 0.003 to 0.051. The observation of two reduction peaks has been reported elsewhere [47] supposedly originating from the reduction of Cr(VI) species in and out of the framework. *In situ* Raman spectroscopy studies performed by Weckhuysen et al. [83] have confirmed two types of surface chromium oxide species on the inorganic oxide: an isolated species which is difficult to be reduced and a polymeric

species which is more easily reduced on the same support. Therefore, the lower and the higher reduction peaks are assumed to be polymeric Cr(VI) oxide and isolated Cr(VI) oxide, respectively. This is explained by the weaker interaction of the polymeric chromium oxide with the support which causes the material to be soluble in water [62, 65, 60]. UV-Vis DRS and FT-IR/ATR results which provide confirmation of a polymerization process also support this conclusion. Here, we use the term "soft Cr(VI)" and "hard Cr(VI)" to refer to easily reducible Cr(VI) oxide and difficultly reducible Cr(VI) oxide, respectively. Cr-MSU-x82 shows another reduction peak at over 500 $^{o}$C which is assigned to α-$Cr_2O_3$. Zhang et al. reported on the reduction of α-$Cr_2O_3$ at a higher temperature than the isolated or polymeric chromium oxide [53]. $H_2$ consumption per gram of catalyst and the ratio of $H_2$/Cr are presented in Table 2-2. The amount of consumed $H_2$ increases until the Cr/Si molar ratio reaches 0.051 and decreases in Cr-MSU-x82 sample. This is caused by that α-$Cr_2O_3$ is dominant in Cr-MSU-x82 sample. The ratio of $H_2$/Cr allows one to estimate the amount of redox Cr(VI) species in the fresh Cr-MSU-xN catalysts. The area for soft and hard Cr(VI) were calculated from the deconvoluted Gaussian lines from the normalized reduction peaks as seen in Table 2-2. The area of the soft Cr(VI) reaches maximum up to Cr-MSU-x14 and Cr-MSU-x28 catalysts and then decreases. The hard Cr(VI) area is largely increased, as the Cr/Si molar ratio increases to 0.01 and decreases slightly until the Cr/Si molar ratio reaches 0.028 and drastically increases again at a Cr/Si molar ratio of 0.051. The ratio of soft Cr(VI) to total Cr(VI) is the highest for the Cr-MSU-x28 catalyst. This

indicates that the Cr-MSU-x28 catalyst contains mainly polymeric Cr(VI) oxides together with isolated Cr(VI) oxide as a minor phase and the soft Cr(VI) might undergo redox processes quite effectively.

### 2.3.4 Catalytic performance

Figure 2-9 shows time on stream catalytic activity with respect to catalytic reaction temperature; 400, 500, 600, and 700 $^{o}$C. The catalytic activity increases linearly with increasing temperature. Selectivity, however, drops dramatically at a reaction temperature of 700 $^{o}$C. The use of $CO_2$ in the dehydrogenation of the propane instead of $O_2$ is to enhance the selectivity of the reaction for propylene as referred to above. Thus, both a high activity and acceptable selectivity is achieved at 600 $^{o}$C, and this is considered to be the most suitable reaction temperature. The catalytic performance of the Cr-MSU-xN catalysts for the dehydrogenation of propane using $CO_2$ was therefore examined at 600 $^{o}$C. In a blank experiment without catalyst at 600 $^{o}$C, propane conversion was 20% and the selectivity for propylene was 50% which corresponds to a 10% yield.

In order to investigate the contribution of $CO_2$ in ODHP reaction, catalytic tests using $C_3H_8$:$N_2$ and $C_3H_8$:$CO_2$:$N_2$ feeds were compared. The results shown in Figure 2-10 clearly indicate that the presence of $CO_2$ markedly improved the yield of propylene. This catalytic performance can be evidence that $CO_2$ plays the promoting role in the conversion of propane to propylene over Cr-MSU-xN catalysts. This promoting effect can be rationalized that

$CO_2$ can play a role in the consumption of $H_2$ produced by the dehydrogenation of propane via a reverse water gas shift reaction. The reaction can be given as follows;

$$C_3H_8 \rightleftharpoons C_3H_6 + H_2 \quad \cdots\cdots (3\text{-}3)$$

$$CO_2 + H_2 \rightleftharpoons CO + H_2O \quad \cdots\cdots (3\text{-}4)$$

The reduction of the partial pressure of hydrogen shifts the dehydrogenation equilibrium towards propylene and CO formation. From the GC data, the correlation between CO area and propylene yield with respect to Cr/Si molar ratio was plotted. The CO area increases with an increase in the Cr/Si molar ratio up to 0.028 and then decreases slightly with further Cr/Si molar ratio which has similar correlation with catalytic activity. It can therefore be concluded that the $CO_2$ has a promotional effect in ODHP reaction by participating in the RWGS reaction and that soft Cr(VI) is mainly responsible for this reaction.

Time-on-stream behavior for catalytic activity over the Cr-MSU-x catalysts series is shown in Figure 2-11. During the 2-hour catalytic reaction, propane conversion and propylene yield decreased within 10 percent while selectivity ranged between 80 and 90 percent with little change. Figure 2-12 shows the catalytic activity of the Cr-MSU-x28 catalyst with time-on-stream. Propane conversion drops with reaction time and approaches a steady state in 25 h, showing a 30% yield of propylene.

Deactivation was investigated in two ways, (i) coke formation and (ii) a

reduction in active chromium sites. It has been reported that $CO_2$ acts as a soft oxidant which reduces the coke deposition by the reverse Boudouard reaction ($CO_2 + C \rightarrow 2CO$) and regenerates the reduced active Cr(III) sites [20, 31]. The amount of coke deposited on the catalyst before and after ODHP reaction over Cr-MSU-x28 catalyst was analyzed. After 120 min over the ODHP reaction, 1.1 wt.% of coke was deposited, which is not sufficiently significant to cause rapid deactivation.

To investigate the effect of the reduction of active chromium sites during the ODHP reaction on the catalyst deactivation, over-reduction was applied on Cr-MSU-x28 catalyst under a 10% of $H_2$/Ar gas stream (50 $cm^3$ $min^{-1}$) at 650 $^oC$ for 3h. After the over-reduction of the Cr-MSU-x28 catalyst, the initial ODHP catalytic activity was decreased. This result strongly supports the conclusion that the main cause of initial catalytic deactivation is the reduction of active chromium sites. Even after the rapid deactivation, the catalytic activity was slowly decreased again. Shishido et al. [68] observed that the $Cr(VI)O_4$ tetrahedron were reduced to $Cr(III)O_6$ octahedron and then converted to an aggregated form of the $Cr(III)O_6$ octahedron during the reaction using Cr K-edge XAFS spectroscopy. It appears that the aggregation of $Cr(III)O_6$ species can cause another decrease in the activity. The regenerative cycles of Cr-MSU-x28 catalyst are represented in Figure 2-13. The propylene yield on the catalyst decreases from 40% to 30% after 120 min on stream in the 1$^{st}$ cycle. The regeneration step was carried out with an air stream at 650 $^oC$ for 3h to re-oxidize the reduced active chromium species. After the regeneration step, the propylene yield was 40% which is the initial

value, indicating that the original activity of the catalyst was fully recovered.

The relation between initial catalytic activity and Cr/Si molar ratio is shown in Figure 2-14. Propylene yields show a similar trend with propane conversion, due to the nearly constant selectivity for propylene regardless of the amount of chromium in the samples. The conversion of propane and the yield of propylene increases steeply with increasing amounts of chromium and reach a maximum at a Cr/Si molar ratio of 0.028. The existence of a maximum in catalytic performance indicates that an optimum Cr/Si molar ratio exists. A further amount of chromium results in a decrease in both the conversion of propane and the yield of propylene. This can be explained by formation of less active, crystalline $\alpha$-$Cr_2O_3$ as confirmed by XRD, UV-Vis DRS, and FT-IR/ATR. In addition, the activity of the Cr-MSU-x28 was compared with that of a reference catalyst prepared by incipient wetness impregnation but containing the same amount of chromium (Figure 2-15). The Cr-MSU-x28 catalyst shows about a 10 percent higher propylene yield which demonstrates the superiority of the prepared Cr-MSU-x catalysts.

The TPR experiment for the $CrO_x$/MSU-x catalyst is conducted. In agreement with the previous $H_2$-TPR results (Figure 2-8), $CrO_x$/MSU-x catalyst shows three distinct reduction peaks which can be attributed to soft Cr(VI) and hard Cr(VI) as well as $\alpha$-$Cr_2O_3$. Although the composition of soft Cr(VI) in total Cr(VI) appears to be high, the negative effect arising from $\alpha$-$Cr_2O_3$ which is difficult to reduce, is more dominant, as evidenced by ODHP catalytic activity.

Determining the active site in chromium oxide has been a research goal

for many years [69]. It has been revealed that the active site of chromium oxide in dehydrogenation reactions is a coordinatively unsaturated Cr(III) ion, as evidenced by *in situ* UV-Vis DRS/ESR [70, 71], UV-Vis DRS/Raman [72, 73], and FT-IR findings [74]. More specifically, Cr(III) ions can be classified into three types: Cr(III) ions formed by reduction of Cr(VI), dispersed Cr(III) ions as isolated center, and small Cr(III) clusters [69]. Among those classified Cr(III) ions, it appears that Cr(III) ions formed by reduction of Cr(VI) plays a major role as an active sites, in agreement with other investigators [47, 75]. However, these investigators did not mention any classified pre-reduced Cr(VI) species i.e. isolated Cr(VI) and polymeric Cr(VI). Since it has been almost impossible to discriminate between the individual contribution of these two types of Cr(VI) species to the overall catalytic activity [50].

The TPR characterization results, in combination with the catalytic activity data, allow a detailed discussion of the nature of the active Cr(VI) species in the oxidative dehydrogenation of propane. The correlation between catalytic activity and the ratio of soft/total Cr(VI) is plotted in Figure 2-16a as a function of the Cr/Si molar ratio. Interestingly, they show similar trend, confirming the importance of the ratio between soft and total Cr(VI). For the clarity of presentation, this relationship is presented in Figure 2-16b. Based on this graph, the composition of the soft Cr(VI) in the Cr-MSU-x catalysts appears to be a key factor for achieving a high performance in the oxidative dehydrogenation of propane. The correlation between the ratio of hard/total Cr(VI) area and the ODHP reaction activity of Cr-MSU-

xN catalysts is presented in Figure 2-16c. As seen in the figure, the composition of hard Cr(VI) in total Cr(VI) has a negative effect on the ODHP catalytic activity.

Shishido et al. [68] proposed the dehydrogenation of propane reaction mechanism in the absence and presence of $CO_2$. In the case of ODHP reaction, oxidative dehydrogenation of propane proceeds through the reduction of Cr(VI) to Cr(III) in the initial stage of the reaction. After the initial stage of the reaction, the formed Cr(III) can also take part in direct dehydrogenation of propane. A part of Cr(III) can be oxidized to Cr(VI) and the reaction cycle can be formed. Taking assume that propylene is produced simultaneously over Cr(VI) and Cr(III), three factors could have affected high performance in the oxidative dehydrogenation of propane; (i) in the initial stage of the reaction, soft Cr(VI) which is more easily reducible to Cr(III) than hard Cr(VI) leads to higher yield of propylene through the oxidative dehydrogenation of propane, (ii) as the multinuclear Cr(III) originated from soft Cr(VI) exhibits higher turnover frequency than isolated Cr(III) site [76], the dehydrogenation of propane on multinuclear Cr(III) would undergo more effectively, and (iii) Cr(III) originated from soft Cr(VI) can be more easily oxidized to Cr(VI) and take part in reaction cycle again. On the basis of these results, we conclude that composition of soft Cr(VI) in the Cr-MSU-x catalysts would be an important factor in the oxidative dehydrogenation of propane due to the effective participation of soft Cr(VI) in the redox cycle.

**Table 2-1.** Physicochemical properties of the pure MSU-x and Cr-MSU-xN catalysts.

| Catalyst* | Cr (wt.%) | Si (wt.%) | Cr/Si molar ratio | Surface area ($m^2 g^{-1}$) | Average pore Size (nm) | Pore volume ($cm^3 g^{-1}$) |
|---|---|---|---|---|---|---|
| Pure MSU-x | - | - | - | 876 | 4.8 | 1.06 |
| Cr-MSU-x3 | 0.18 | 26.07 | 0.003 | 903 | 4.5 | 1.03 |
| Cr-MSU-x10 | 0.46 | 26.67 | 0.010 | 896 | 4.1 | 0.93 |
| Cr-MSU-x14 | 0.62 | 22.80 | 0.014 | 848 | 4.2 | 0.90 |
| Cr-MSU-x28 | 1.27 | 24.44 | 0.028 | 791 | 4.5 | 0.88 |
| Cr-MSU-x51 | 2.16 | 22.98 | 0.051 | 754 | 4.2 | 0.78 |
| Cr-MSU-x82 | 3.59 | 23.79 | 0.082 | 730 | 3.9 | 0.71 |

*Cr-MSU-xN, where N indicates the Cr/Si molar ratio multiplied by $10^3$.

**Table 2-2.** Reducibility of the Cr-MSU-xN catalysts from $H_2$-TPR profiles.

| Catalyst[a] | $H_2$ consumption ($mmol \cdot g^{-1}$) | $H_2$/Cr | Soft Cr(VI) Area[b] | Hard Cr(VI) Area[b] | Soft/Total Cr(VI) Area |
|---|---|---|---|---|---|
| Cr-MSU-x3 | 0.046 | 1.33 | 0.08 | 0.84 | 0.089 |
| Cr-MSU-x10 | 0.14 | 1.55 | 0.15 | 1.16 | 0.12 |
| Cr-MSU-x14 | 0.21 | 1.73 | 0.35 | 1.08 | 0.25 |
| Cr-MSU-x28 | 0.30 | 1.21 | 0.32 | 0.72 | 0.30 |
| Cr-MSU-x51 | 0.76 | 1.83 | 0.22 | 1.27 | 0.15 |
| Cr-MSU-x82 | 0.46 | 0.67 | 0.06 | 0.46 | 0.12 |

[a]Cr-MSU-xN, where N indicates the Cr/Si molar ratio multiplied by $10^3$.

[b]Soft and hard Cr(VI) area was calculated from the deconvoluted Gaussian lines from the normalized reduction peaks (Figure 2-8).

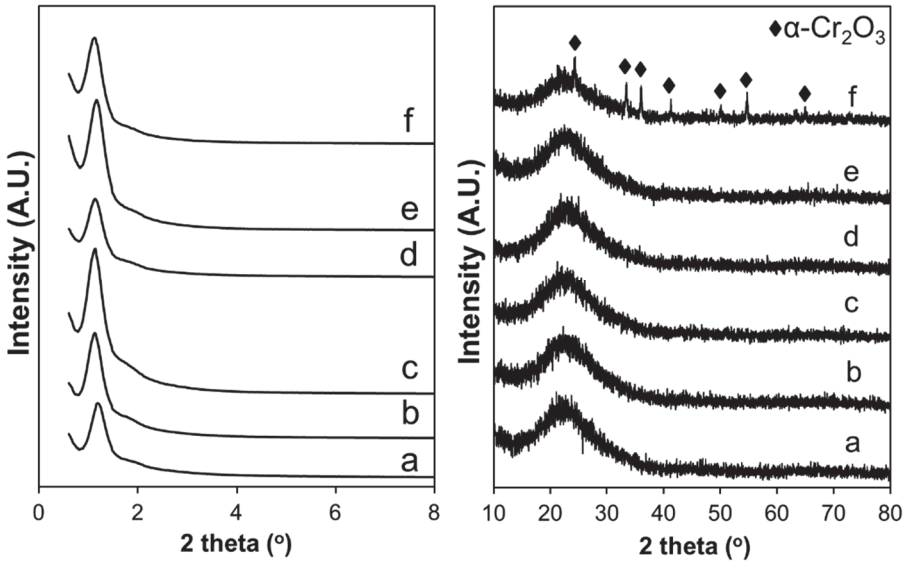


**Figure 2-1.** XRD powder patterns of Cr-MSU-xN catalysts: (a) Cr-MSU-x3; (b) Cr-MSU-x10; (c) Cr-MSU-x14; (d) Cr-MSU-x28; (e) Cr-MSU-x51; (f) Cr-MSU-x82.

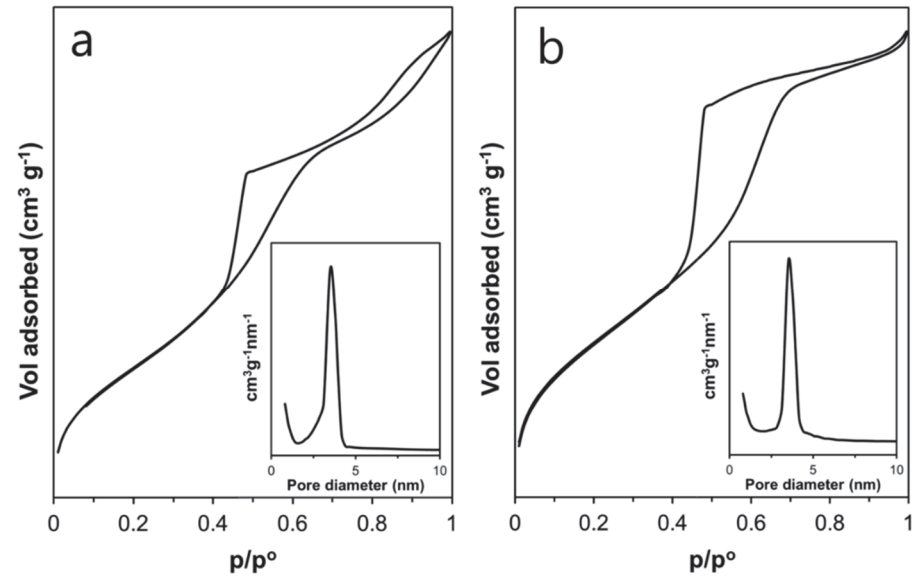


**Figure 2-2.** $N_2$ adsorption-desorption isotherms and pore size distributions of (a) pure MSU-x and (b) Cr-MSU-x51 materials.

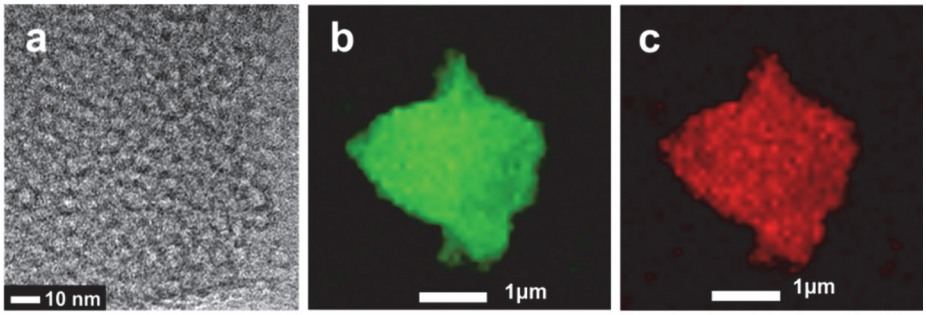


**Figure 2-3.** Morphological and compositional studies of Cr-MSU-x51 catalyst obtained by microscopy techniques. (a) HR-TEM image of Cr-MSU-51. And 2-D atomic mapping by using analytical STEM equipped with EDS; (b) Si and (c) Cr.

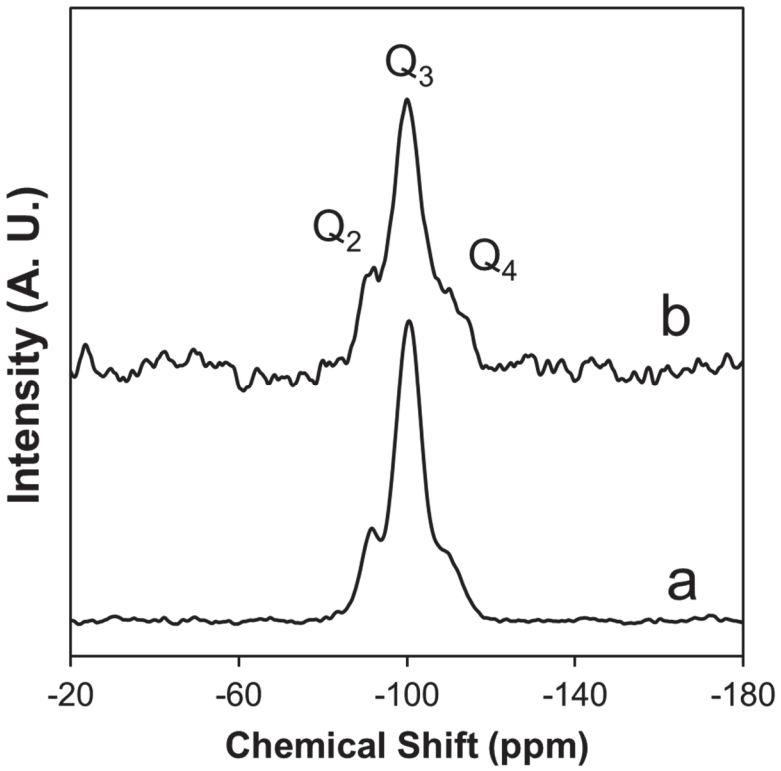


**Figure 2-4.** $^{29}$Si MAS NMR spectra of the (a) pure MSU-x and (b) Cr-MSU-x28 materials.

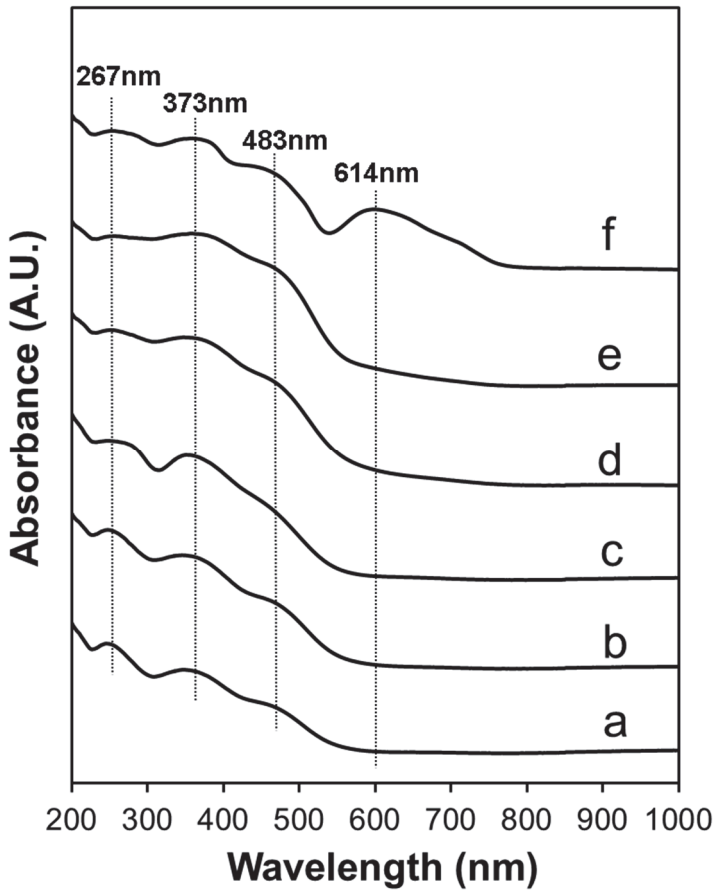


**Figure 2-5.** Diffuse reflectance UV-Vis spectra of Cr-MSU-xN catalysts: (a) Cr-MSU-x3; (b) Cr-MSU-x10; (c) Cr-MSU-x14; (d) Cr-MSU-x28; (e) Cr-MSU-x51; (f) Cr-MSU-x82.

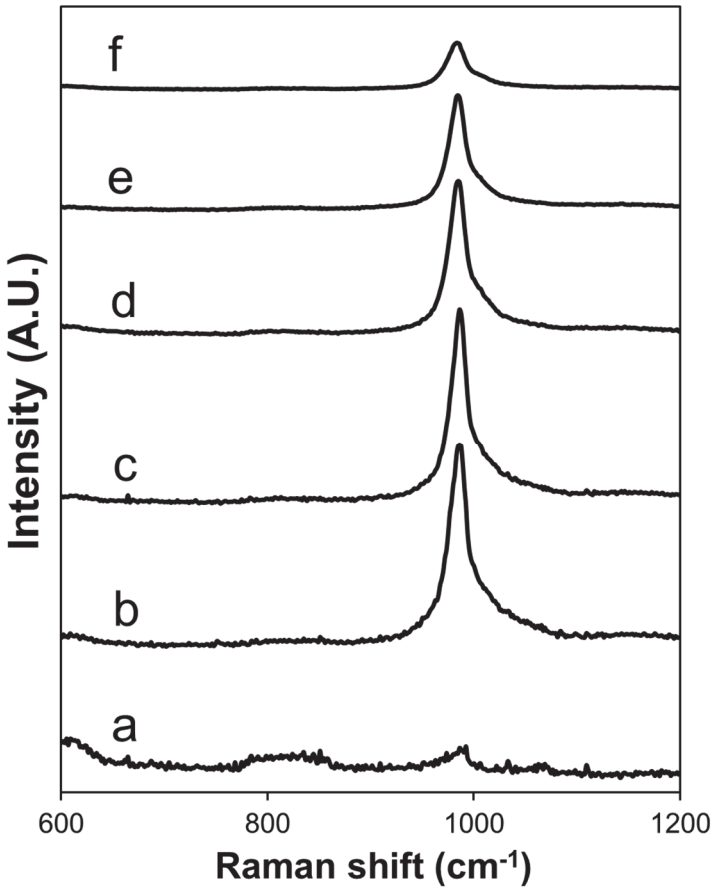


**Figure 2-6.** UV-Raman spectra of Cr-MSU-xN catalysts: (a) Cr-MSU-x3; (b) Cr-MSU-x10; (c) Cr-MSU-x14; (d) Cr-MSU-x28; (e) Cr-MSU-x51; (f) Cr-MSU-x82.

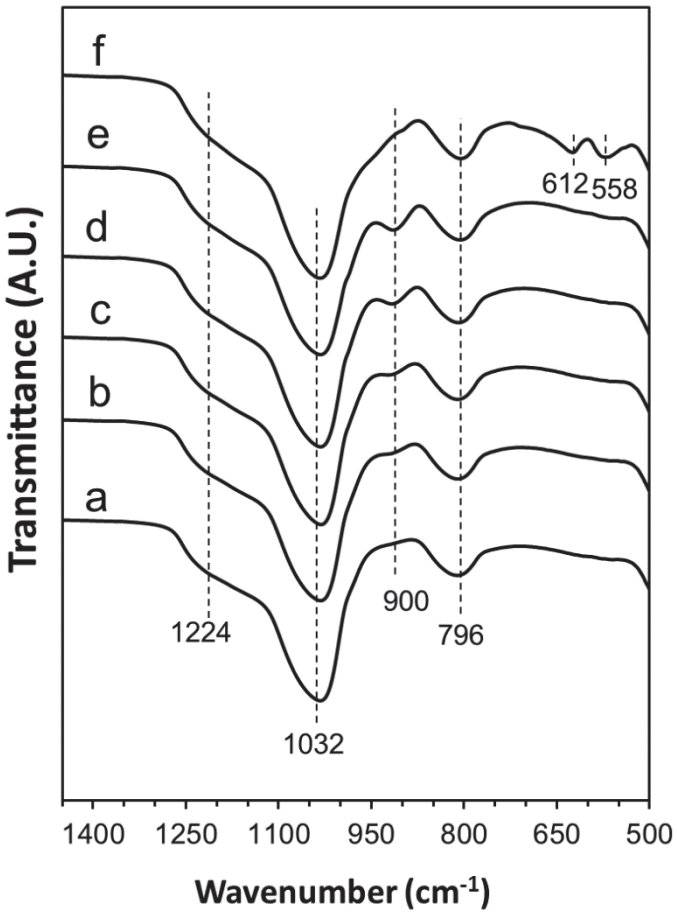


**Figure 2-7.** FT-IR/ATR spectra of Cr-MSU-xN catalysts: (a) Cr-MSU-x3; (b) Cr-MSU-x10; (c) Cr-MSU-x14; (d) Cr-MSU-x28; (e) Cr-MSU-x51; (f) Cr-MSU-x82.

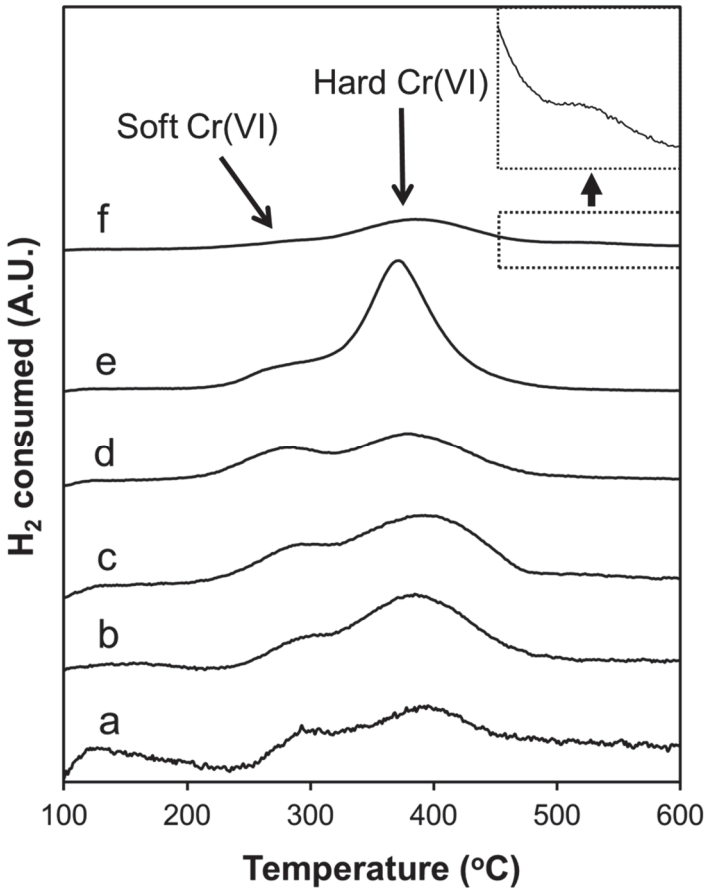


**Figure 2-8.** $H_2$-TPR profiles of Cr-MSU-xN catalysts: (a) Cr-MSU-x3; (b) Cr-MSU-x10; (c) Cr-MSU-x14; (d) Cr-MSU-x28; (e) Cr-MSU-x51; (f) Cr-MSU-x82.

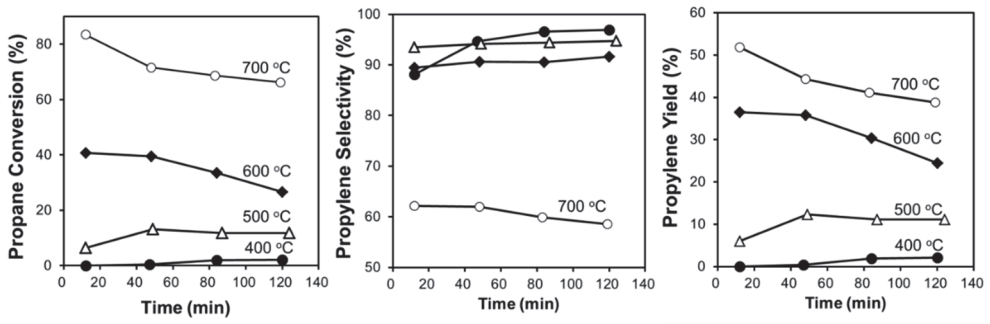


**Figure 2-9.** Time on stream for propane conversion, selectivity and propylene yield over Cr-MSU-x28 catalyst at various ODHP reaction temperatures: (●) 400 ºC; (△) 500 ºC; (◆) 600 ºC; (○) 700 ºC.

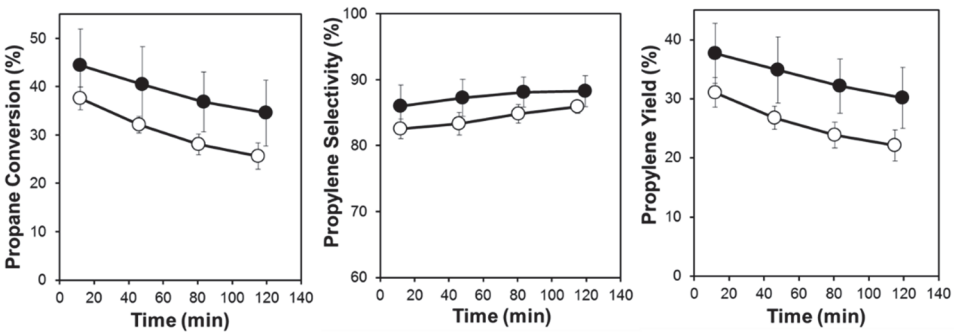


**Figure 2-10.** Time on stream for propane conversion, selectivity and propylene yield over Cr-MSU-x28 catalysts: (●) Oxidative dehydrogenation of propane using $CO_2$; (○) Direct dehydrogenation of propane without $CO_2$.

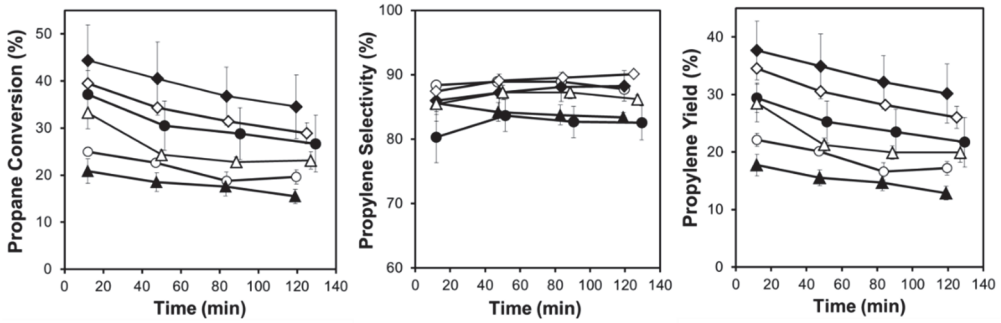


**Figure 2-11.** Time on stream for propane conversion, selectivity and propylene yield over Cr-MSU-xN catalysts: (▲) Cr-MSU-x3; (○) Cr-MSU-x10; (●) Cr-MSU-x14; (◆) Cr-MSU-x28; (◇) Cr-MSU-x51; (△) Cr-MSU-x82.

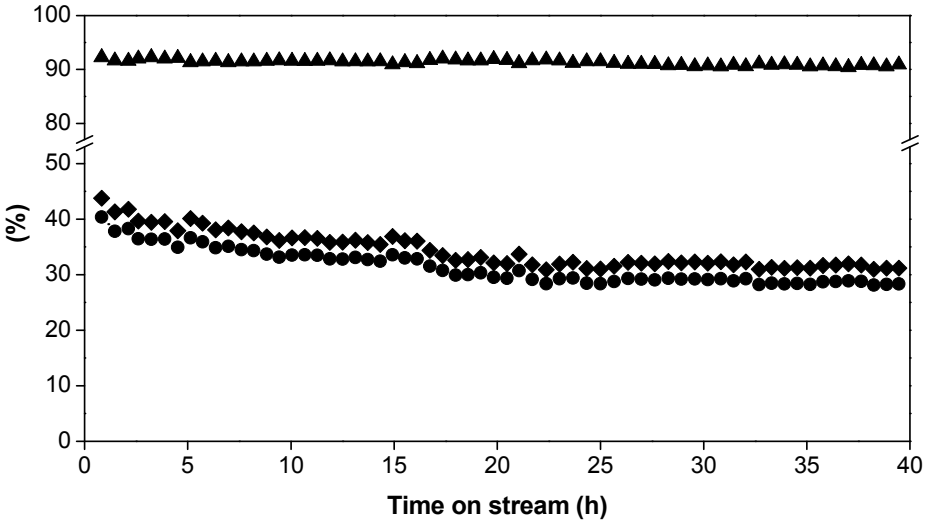


**Figure 2-12.** Propane conversion (◆), propylene selectivity (▲), and propylene yield (●) for Cr-MSU-x28 catalyst as a function of reaction time.

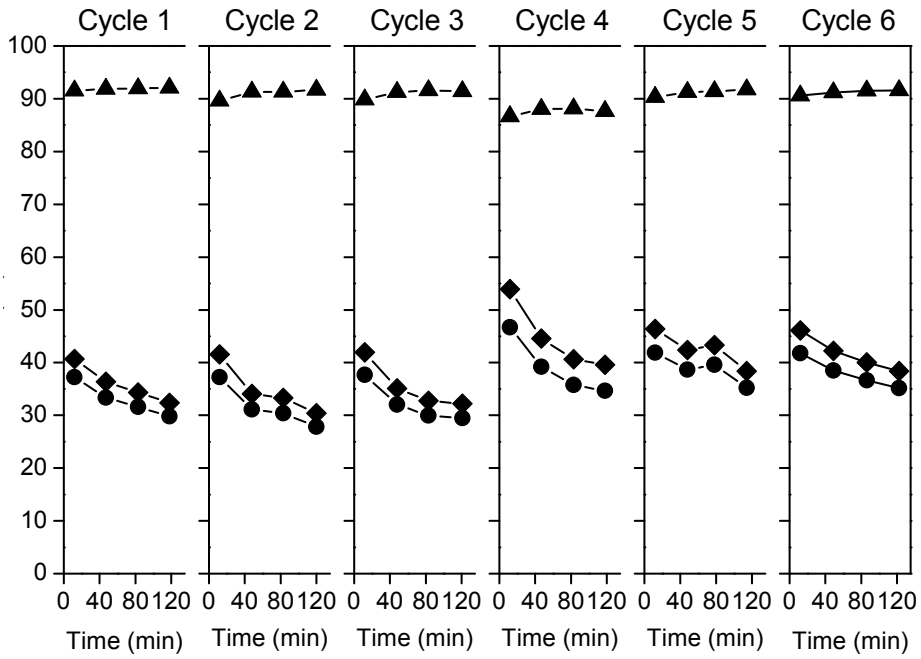


**Figure 2-13.** Regeneration treatment of the Cr-MSU-x28 catalyst with air at 650 $^{o}$C for 3 h; propane conversion (◆), propylene selectivity (▲), and propylene yield (●).

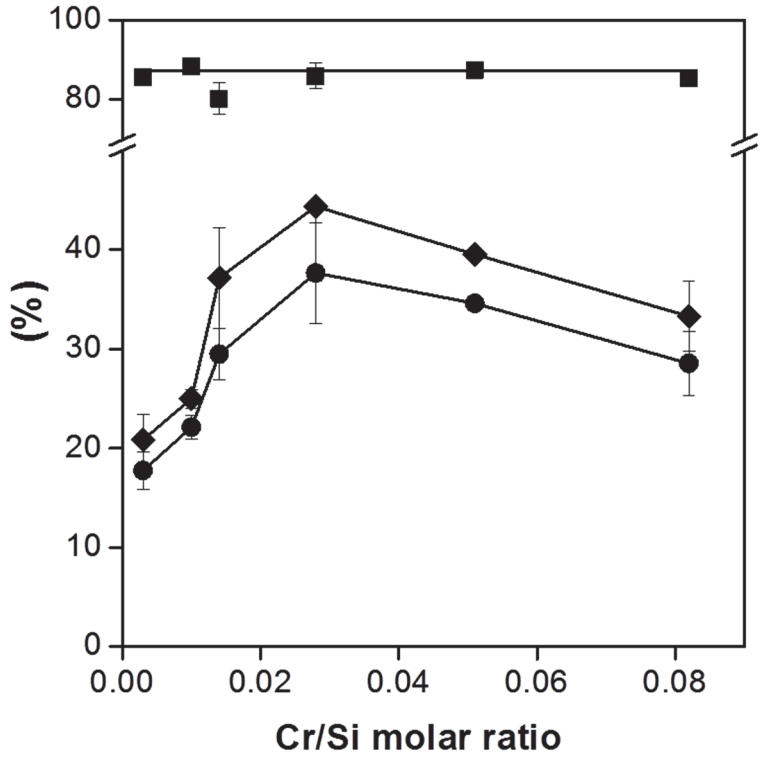


**Figure 2-14.** Variation in propane conversion, selectivity and propylene yield over Cr-MSU-xN catalysts: (◆) propane conversion; (▲) propylene selectivity; (●) propylene yield.

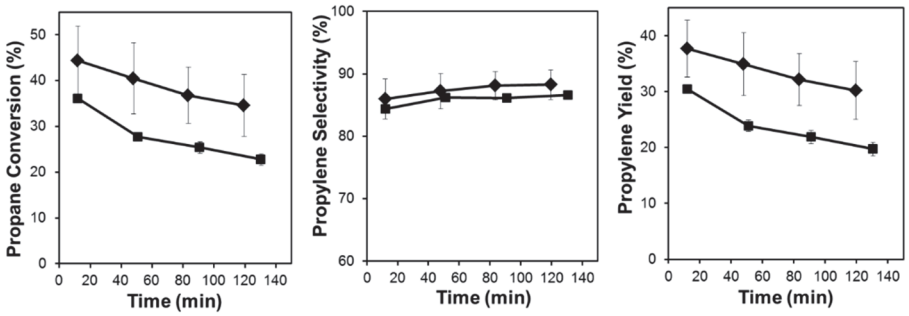


**Figure 2-15.** Comparison of propane conversion, selectivity and propylene yield over the Cr-MSU-xN and $CrO_x$/MSU-x catalysts: (◆) Cr-MSU-x28; (■) $CrO_x$/MSU-x.

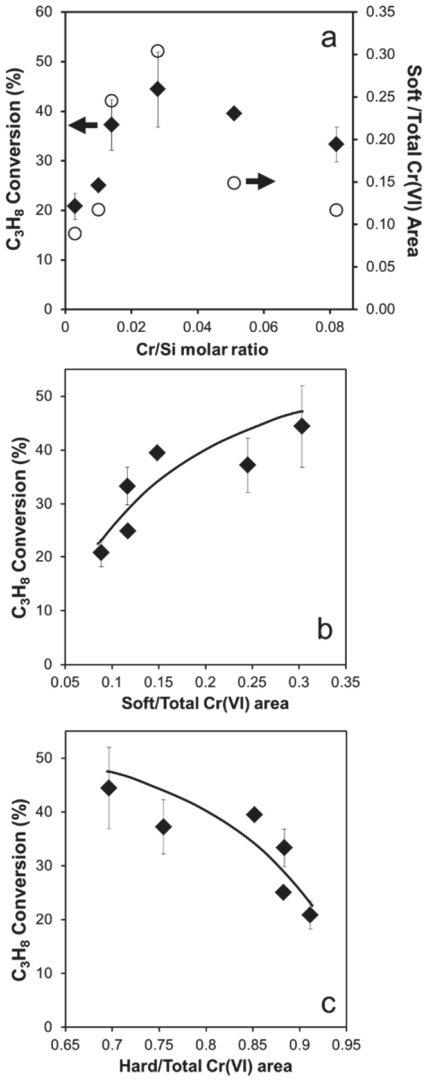


**Figure 2-16.** (a) Relationship between the ratio of soft/total Cr(VI) area and initial ODHP reaction activity with respect to Cr/Si molar ratio in Cr-MSU-xN catalysts; (b) Correlation between the ratio of soft/total Cr(VI) area and initial ODHP reaction activity of Cr-MSU-xN catalysts; (c) Correlation between the ratio of hard/total Cr(VI) area and initial ODHP reaction activity of Cr-MSU-xN catalysts.

# Chapter 3. Addition of Ni as a Co-Catalyst for the Regeneration of Chromium Active Site in Oxidative Dehydrogenation of Propane using $CO_2$

## 3.1 Introduction

Propylene can serve as a precursor for the production of valuable products such as cumene, acrylonitrile, propylene oxide and polypropylene [77, 78]. Among the processes used in the synthesis of propylene, the oxidative dehydrogenation of propane using $CO_2$ (ODHP) has received considerable attention, since it involves the utilization of the greenhouse gas, $CO_2$ [79, 80]. Typically, most efforts have concentrated on the utilization of $CO_2$ as an attractive C1 building block. However, it has recently been proposed that $CO_2$ might also be utilized as an oxygen transfer agent or as a soft oxidant [81]. By using $CO_2$ as a soft oxidant in the ODHP reaction, coke deposition can be eliminated and the reduced active phase can be re-oxidized [82, 83].

$CrO_x$/silica is considered as promising materials due to its high activity among the active materials in the ODHP reaction [84, 85]. Active sites of $CrO_x$ are reported to be coordinatively unsaturated Cr(III) in chromium species in dehydrogenation reactions [86, 87]. Accordingly, several groups reported that Cr(III) formed from the reduction of higher-valence states, i.e.

Cr(VI), are active sites in dehydrogenation reaction [88, 89]. This is supported by the evidence that higher-valence chromium states are instantly reduced when in contact with alkanes at high temperature [90]. Despite its high activity, $CrO_x$/silica catalysts suffer from 'rapid deactivation' [91]. The reasons for the deactivation of $CrO_x$/silica catalysts are thought to be coke deposition and the reduction of $CrO_x$; to convert the coordinatively unsaturated Cr(III) state into the inactive Cr(II) state [90-92]. A study had directed at the behavior of active sites on $CrO_x$/silica catalysts during the ODHP reaction using $CO_2$ reported [93] that the $C_3H_8$ conversion of Cr/Cab-O-Sil was not recovered, even when the effects of coke were eliminated. Consequently, this implies that the main factor in the deactivation of $CrO_x$/silica catalysts is related to the reduction of $CrO_x$.

K. Nakagawa et al. [94] reported that the state of the surface chromium remained in a higher oxidation state in the presence of $CO_2$ than in its absence in the oxidative dehydrogenation of lower alkanes. However, it was pointed out that $CO_2$ has limited oxidizing ability, in terms of re-oxidizing the reduced $CrO_x$, due to its thermodynamically stable properties [95]. The oxidizing power can be improved by the addition of $O_2$ in the reactant as a co-feed with $CO_2$. The deactivation rate of the $CrO_x$/silica catalyst was diminished by the addition of a small amount of $O_2$ [96]. Unfortunately, the selectivity of the reaction for $C_3H_6$ was significantly decreased. Therefore, the development of a suitable promoter to activate $CO_2$ which would enhance the oxidizing ability of $CO_2$ and also maintain a stable selectivity for propylene would be highly desirable.

Nickel (Ni)-based catalysts are widely used in $CO_2$ reforming reactions [97-99] and the reverse water gas shift reaction (RWGS) [100]. Such catalysts have an excellent ability to activate $CO_2$, even under harsh reaction conditions. Alexander M. Mebel et al. [101] reported that the activation energy for the dissociation of $CO_2$ on Ni atoms is significantly lowered than that for $CO_2$ in the absence of Ni atoms via ab-initio calculations. Choe et al. [102] studied the adsorption and dissociation of $CO_2$ by a molecular orbital method on Ni(111) within a 25-atom cluster. The strong chemisorption of $CO_2$ on Ni leads to the bending of the molecule because the d metal is mixed with $2\pi_u$ in the $CO_2$ orbital to form $6a_1$. The chemisorbed $CO_2$ undergoes a sequential carbon-oxygen bond cleavage to generate CO and activated O ($O^*_{ads}$). Such $O^*_{ads}$ generated on Ni could play a role in the re-oxidation of the reduced $CrO_x$ species during the ODHP reaction. The regenerated $CrO_x$ could act as active sites in the ODHP reaction which leads to reduce deactivation of catalyst.

In this work, we report on the preparation of a Ni promoted $CrO_x$/SBA-15 catalyst by a sequential impregnation method in order to decrease deactivation of catalyst in the ODHP reaction. The 10 wt.% $CrO_x$/SBA-15 and Ni promoted 10 wt.% $CrO_x$/SBA-15 samples were designated as Cr/Si and #Ni-Cr/Si, respectively where # indicates the weight of Ni loading. We expected that Ni enhances oxidizing ability of $CO_2$ to re-oxidize reduced Cr(II) state to active Cr(III) state and also Cr(III) to Cr(VI). To verify the effect of Ni, 3-step $H_2$-temperature programmed reduction (TPR) and *ex situ* X-ray photoelectron spectroscopic (XPS) experiments were carried out.

## 3.2 Experimental

### 3.2.1 Preparation of Ni-Cr/$SiO_2$ catalysts

The synthesis of SBA-15 was prepared as described in a previous report, with minor modifications [103]. A poly(ethylene glycol)-block-poly(propylene glycol)-block-poly(ethylene glycol) (3.27 g, $EO_{20}PO_{70}EO_{20}$, P123, average molecular weight = 5800, Aldrich) was dissolved in deionized water (100 ml). A solution of HCl (8.6 mL, 37%, SAMCHUN Chemical) and tetraethyl orthosilicate (6.9 ml, TEOS, > 99%, Aldrich), a silicon source, was added. The mixture was stirred at 40 $^{o}$C for 24 h and then placed in an oven at 100 $^{o}$C for 24 h without stirring. The synthesized material was isolated on a filter, washed with deionized water and dried at room temperature. The resulting powder was calcined at 550 $^{o}$C for 4 h. 10 wt.% $CrO_x$/SBA-15 sample (Cr/Si) and Ni promoted samples (#Ni-Cr/Si, where # indicates loading weight of Ni) were prepared by the incipient wetness impregnation method. The Ni promoted samples were also prepared by the sequential impregnation method. The SBA-15 was impregnated with an aqueous solution of chromium nitrate nonahydrate ($Cr(NO_3)_3 \cdot 9H_2O$, 98%, SAMCHUN Chemical). After the impregnation, the samples were dried for 12 h at 80 $^{o}$C and calcined at 650 $^{o}$C for 3 h. Subsequently, 10 wt.% $CrO_x$/SBA-15 was impregnated by exposure in an aqueous solution of nickel chloride ($NiCl_2 \cdot 6H_2O$, Hayashi pure chemical) with a NiO content of 0.1, 0.5,

and 1 wt.%. The drying and calcination steps were the same as for the 10 wt.% $CrO_x$/SBA-15 sample.

### 3.2.2 Characterization of Ni-Cr/$SiO_2$ catalysts

The X-ray diffraction (XRD) patterns were obtained in two ranges of 1-10$^o$ and 10-80$^o$ using a SAXS with GADDS and Rigaku D-MAX2500-PC powder X-ray diffractometer, respectively, with Cu Kα radiation (1.5406 Å). The $N_2$ adsorption-desorption isotherms were recorded on a Micrometrics ASAP-2010 system. The total surface area of the samples was determined by the BET method. The pore volume and pore area distributions were calculated from the adsorption branches of the isotherms using BJH methods. High resolution transmission electron micrograph (HR-TEM) images were obtained with a JEOL JEM-3010 microscope with the acceleration voltage of 300 kV. In order to explore the mapping of elemental distribution on the samples, an analytical high-angle annular dark-field scanning transmission electron microscope (HAADF-STEM, Tecnai F20-FEI, 200 kV) equipped with energy dispersive X-ray spectroscopy (EDS, Tecnai 136-5-EDAX) was used. UV-Vis diffuse reflectance spectroscopy measurements were recorded on the Jasco V670 spectrometer with diffuse reflectance spectroscopy (DRS) unit. The spectra were collected at 200-1000 nm referenced to KBr. The amount of coke deposited on the catalyst was determined by CHNS analysis (CHNS-932, LECO). Temperature-programmed reduction (TPR) results were obtained using a Micromeritics Autochem II chemisorption analyzer.

Importantly, in order to investigate the effect of Ni on activating $CO_2$, TPR typically involved 3 steps. First, the samples were pretreated at 150 $^oC$ for 30 min in a flow of He (50 $cm^3 \cdot min^{-1}$) and cooled down to 50 $^oC$. The TCD signal was then recorded with increasing temperature up to 700 $^oC$ at a rate of 10 $^oC \cdot min^{-1}$ under a flow of 10 % $H_2$/Ar (50 $cm^3$ $min^{-1}$). Secondly, to insure the total reduction of the sample, the same TPR procedure was conducted with reduced samples from the first step. Thirdly, the samples were treated under a flow of $CO_2$ (50 $cm^3$ $min^{-1}$) at 600 $^oC$ for 1h. After cooling down to 50 $^oC$, the TCD signal was recorded again with increasing temperature up to 700 $^oC$ at a rate of 10 $^oC \cdot min^{-1}$ under a flow of 10 % $H_2$/Ar (50 $cm^3$ $min^{-1}$). X-ray photoelectronspectroscopy (XPS) experiments were carried out on an SIGMA PROBE (ThermoVG, U.K) instrument. The binding energy of each element was calibrated using the carbon peak as the standard (C 1s = 284.5 eV). For *ex situ* XPS experiments, the catalysts were collected after the desired reaction time. The collected samples were processed as in the form of a pellet for the analysis.

### 3.2.3 Catalytic reactions

The oxidative dehydrogenation of propane using $CO_2$ reaction was performed in a flow-type quartz reactor under atmospheric pressure at a temperature of 600 $^oC$. A 0.2 g sample of catalyst was loaded in the reactor and the catalyst was preheated from room temperature to 600 $^oC$ in a flow of $N_2$ (30 $cm^3$ $min^{-1}$). The reaction gas stream consisted of $C_3H_8$, $CO_2$, and $N_2$

with a volumetric ratio of 1:1:8, at a total flow rate of 30 $cm^3 \cdot min^{-1}$. The products were analyzed using an on-line gas chromatograph (Donam DS 6200) equipped with a flame ionization detector (FID) and a thermal conductivity detector (TCD). $CO_2$ and $C_2$-$C_3$ hydrocarbons were separated in a column packed with the Porapak Q whereas $N_2$, CO and $C_1$ were separated using a molecular sieve. FID and TCD were used for quantification of $C_1$-$C_3$ hydrocarbons and non-hydrocarbons ($N_2$, CO, and $CO_2$), respectively.

## 3.3 Results and discussion

### 3.3.1 Effect of added Ni on the physicochemical properties

The effect of Ni addition by the sequential impregnation method was examined. In order to confirm physicochemical properties of the prepared catalysts, XRD, SAXS, HR-TEM, HAADF-STEM, $N_2$ adsorption-desorption, and UV-Vis DRS experiments were performed.

XRD patterns for the catalysts are shown in Figure 3-1. The broad peak between 15° and 30° is characteristic of amorphous silica, i.e., the SBA-15 support. For both of the 0.5Ni-Cr/Si and Cr/Si catalysts, diffracted peaks were observed at 2θ = 24.5, 33.6, 36.2, 41.4, 50.2, 54.8, 63.4 and 65.1° which corresponds to (012), (014), (110), (113), (024), (116), (214) and (300) of crystalline α-$Cr_2O_3$, respectively. In the case of 0.5Ni-Cr/Si catalysts, no peak assigned to NiO was observed because the amount of NiO was too small to be detectable or was highly dispersed on the Cr/Si catalyst. XRD patterns for chromium species on both catalysts exhibit similar patterns, indicating that the addition of NiO does not have a significant influence on the crystalline α-$Cr_2O_3$ phase of catalyst.

Small-angle X-ray scattering (SAXS) patterns for the prepared catalysts are shown in Figure 3-2. All the samples show three peaks; (100), (110), and (200) in their corresponding patterns, which are typical two-dimensional hexagonally-ordered mesostructure (*p6mm*) of SBA-15. For the as-calcined SBA-15 sample, the estimated value of $d_{100}$ is 10.0 nm (2θ = 0.88°). Small

shifts of the XRD peaks in Cr/Si and 0.5Ni-Cr/Si to higher angles suggest that the ordered mesostructure slightly shrinked which could be arised by the repeated calcination steps after impregnations of chromium precursor and nickel precursor, respectively. After loading of chromium oxide, the value of $d_{100}$ decreased to 9.4 nm ($2\theta = 0.94^{o}$) and little change of $d_{100}$ value occurred in 0.5Ni-Cr/Si which is corresponding to 9.2 nm ($2\theta = 0.96^{o}$).

$N_2$ adsorption-desorption isotherms of SBA-15, Cr/Si, and 0.5Ni-Cr/Si are shown in Figure 3-3 which exhibits type IV isotherm with H1-type hysterisis for all the samples. The mesoporous structures of all catalysts were well maintained after the addition of the Ni. Structural and textural properties of catalysts obtained by $N_2$ adsorption-desorption analysis and SAXS are shown in Table 3-1. Lattice parameters calculated from $d_{100}$ spacing are decreased in Cr/Si and 0.5Ni-Cr/Si by shift to higher angles of (100) peak in SAXS result. BET surface area, pore volume, and pore size are decreased with the increase in chromium and Ni addition and wall thickness is slightly increased.

HR-TEM image of the Cr/Si is shown in Figure 3-4(a). Highly ordered cylindrical pores of SBA-15 and crystalline α-$Cr_2O_3$ phase in the range of 100-200 nm with irregular shape were observed. Generally, chromium oxide is known to possess various types of chromium species depending on the loading weight of chromium precursor.[27] As the chromium precursor increases chromium species are formed as the following sequence: grafted Cr(VI), dispersed Cr(VI) oxide, microcrystalline Cr(III) oxide, and crystalline α-$Cr_2O_3$. In particular, the final chromium species, α-$Cr_2O_3$, are

builded up over underlying dispersed chromium species after completion of the support coverage [104]. As the most of the crystalline α-$Cr_2O_3$ are larger than the size of the SBA-15 pores, α-$Cr_2O_3$ should be present outside of the SBA-15 pores. Inside the pores of the SBA-15 are expected that grafted Cr(VI), dispersed Cr(VI) oxide, and microcrystalline Cr(III) oxide are monolayerly dispersed. In the case of the 0.5Ni-Cr/Si catalyst (Figure 3-4(b)), NiO was not discriminated from α-$Cr_2O_3$. To investigate the distribution of Ni on Cr/Si samples, an analytical STEM with large angle detection was used for the 2-D mapping of the 0.5Ni-Cr/Si catalyst images, as shown in Figures 3-4(c) and (d). From these 2-D atomic mapping images, it was possible to confirm that chromium oxide and nickel oxide (~30 nm) are located in close proximity to one another on the SBA-15. Therefore, if Ni activates $CO_2$, causing it to dissociate to produce CO and $O^*_{ads}$, the generated $O^*_{ads}$ would be expected to have a greater chance to be transferred to the reduced chromium phase.

Figure 3-5 illustrates the UV-Vis DRS of prepared catalysts. There are four characteristic peaks and three bands centered at 261, 360, and 469 nm which as assigned to Cr(VI) species. Among the referred three peaks, the former two peaks are assigned to a $^1A_1 \rightarrow {}^1T_2$ transition of tetrahedral chromium oxide and the other peak, centered at 469 nm, is assigned to the $^1A_1 \rightarrow {}^1T_1$ transition [105]. The peak at 610 nm corresponds to a $A_{2g} \rightarrow T_{2g}$ charge transfer, which is typical of octahedrally coordinated Cr(III) in α-$Cr_2O_3$ [106]. The UV-Vis DRS results indicate that the prepared catalysts both contain Cr(VI) and Cr(III) species, although Cr(III) species is dominant by α-$Cr_2O_3$. After the addition of

Ni, the overall intensity of the four peaks is slightly decreased. This suggests that the added Ni might affect the chromium species and convert them into other species, such as nickel chromate [107].

### 3.3.2 Effect of Ni on catalytic activity

The prepared Ni promoted Cr/Si catalysts were in the form of NiO and α-$Cr_2O_3$ on SBA-15 after calcination in air. The NiO is, however, reduced to Ni during the first few minutes of the ODHP reaction [108] and is present as an elemental Ni phase during the reaction. Therefore, we focused on the role of Ni itself and not NiO. Time-on-stream catalytic activity with respect to different loading weights of Ni on the Cr/Si catalyst was conducted. The use of 0.1 wt.% Ni had no significant effect on catalytic activity but the yield of propylene was about 5 % higher after 10 h.

The conversion of $CO_2$ and propane increases linearly with increasing loading weight of Ni. When the weight of loaded Ni exceeded 1 wt.%, however, the catalytic reaction favored the dry reforming reaction, which lowered the selectivity for propylene [109]. The maximum promotional effect was observed when 0.5 wt.% Ni was loaded. Based on these data, the catalytic performance of 0.5 wt.% Ni promoted Cr/Si catalyst was the major focus of our investigation.

The ODHP catalytic activities of the catalysts are presented in Figure 3-6. 0.5Ni-Cr/Si and Cr/Si catalyst exhibit quite different trends. At the first point of reaction data, the conversion of $CO_2$ and propane for the 0.5Ni-Cr/Si

catalyst are significantly higher than those of non-promoted catalyst, whereas the selectivity for propylene is nearly zero which leads to zero yield of propylene as well. This suggests that $CO_2$ reforming of propane was preferred to the ODHP reaction early in the reaction. The reaction pathway, however, was fully returned to ODHP reaction after the first cycle.

When the ODHP reaction was dominant, the conversion of $CO_2$ on the 0.5Ni-Cr/Si catalyst was 10% higher than that of non-promoted one. This promotional activation of $CO_2$ was caused by the added Ni on the Cr/Si. The deactivation tendency for the 0.5Ni-Cr/Si catalyst was noticeably lowered than that for the non-promoted one. From the CHNS measurement, the amount of deposited coke was analyzed as shown in Table 3-2. The weight fraction of deposited coke was 12% in Cr/Si, while the value was 16.7% in the case of 0.5Ni-Cr/Si. The amount of deposited coke on the 0.5Ni-Cr/Si was also higher in the carbon balance equation. This result revealed that the deactivation of the Cr/Si catalyst was mainly affected by the transformation of active sites rather than coke deposition. Importantly, Ni played the role to maintain the stable catalytic activity. Higher conversion of $CO_2$ and stable production of propylene implies that Ni dissociates $CO_2$ to CO and $O^*_{ads}$ [110] which could regenerate reduced Cr species, Cr(II), to Cr(III) by re-oxidation.

### 3.3.3 Regeneration of active sites with $CO_2$

The reducibility and regenerating ability of the catalysts were investigated by a 3 step-TPR analysis using $CO_2$. Details of the method are given in the experimental section. In Figure 3-7(a), there are two overlapped peaks in the 1st TPR where the peak shown at the lower temperature and that at a higher temperature correspond to the reduction of polymeric Cr(VI) oxide and isolated Cr(VI) oxide to lower oxidation state of Cr (i.e., Cr(III) and Cr(II)), respectively [111]. In the 2nd TPR, a negligible reduction peak was found, meaning that all chromium states are totally reduced in the 1st TPR. After the treatment of $CO_2$ at 600 $^oC$ for 1 h, a small amount of Cr(VI) was recovered, as shown in the 3rd TPR-$CO_2$.

In the case of the 0.5Ni-Cr/Si catalyst as shown in Figure 3-7(b), the intensity of the 1st TPR peak is decreased and new peaks centered at about 200 $^oC$ and 500 $^oC$ are appeared. This indicates that the chromium phase is transformed after introducing Ni in the Cr/Si catalyst. The peak around 200 $^oC$ is assigned to Cr(VI) which was affected by Ni, as reported by J. B. Wang et al. [112]. Another peak at around 500 $^oC$ is assigned to nickel silicate or a very small amount of NiO [113]. This transformation of the chromium phase is consistent with the UV-Vis DRS results. In the 2nd TPR peak, it appears that the catalysts were entirely reduced in the 1st TPR. Interestingly, in the 3rd TPR peak, a large portion of the 1st TPR peak was recovered after the $CO_2$ treatment. Based on this regenerated 3rd TPR-$CO_2$ peak, it can be concluded

that the reduced Cr(III) and Cr(II) are mainly regenerated to Cr(VI) during the $CO_2$ treatment aided by Ni.

Since the active and inactive states of chromium can be distinguished from *ex situ* XPS data, the role of Ni as a promoter of the reaction was investigated in detail by *ex situ* XPS measurements. $CrO_x$ can be present in various oxidation states; Cr(II), Cr(III), Cr(V) and Cr(VI) [114, 115]. Among the various states, coordinatively unsaturated Cr(III) states, formed from the reduction of higher-valence states, i.e. Cr(VI), are known to be main active sites for the ODHP reaction, while Cr(II) state is active for light alkene polymerization [88, 89, 115, 116]. The $CrO_x$/silica catalyst is active both in the dehydrogenation and the reverse water-gas shift (RWGS) reaction [117]. Ohishi et al. [118] proposed that over the $CrO_x$/MCM-41 catalyst, the RWGS reaction can be proceeded via a redox cycle.

$$Cr(III)\text{-}O^- + H_2 = Cr(II) + H_2O \quad \cdots\cdots (4\text{-}1)$$

$$Cr(II) + CO_2 = Cr(III)\text{-}O^- + CO \quad \cdots\cdots (4\text{-}2)$$

According to this cycle, hydrogen formed during the dehydrogenation of propane reduces Cr(III) to Cr(II) species (4-1), which in the next step is re-oxidized by $CO_2$ (4-2).

XPS analyses of Cr(VI), however, present complexity in the interpretation of the spectra due to the reduction of Cr(VI) by X-ray radiation, as reported by some authors [119, 120]. Therefore, we focused to analyze the presence of active Cr(III) sites which can result in the stable production of propylene.

Figure 3-8 shows *ex situ* XPS spectra of the Cr 2p region with two characteristic peaks centered at about 577.4 and 587.4 eV, corresponding to two Cr $2p_{3/2}$ and Cr $2p_{1/2}$ spin-orbit components, respectively [89, 121]. According to the literature, [114, 121] the binding energy of Cr $2p_{3/2}$ signals at about 577.4 eV could be assigned to the Cr(III) state and that of 575.9 eV to the Cr(II) state. The intensity of the spectra for both catalysts during the ODHP reaction was decreased due to the deposition of coke on the surface of the catalysts. This effect was more pronounced in the case of the 0.5Ni-Cr/Si catalysts by the early dry reforming reaction step. Both fresh catalysts, before the ODHP reaction, show the presence of a Cr(III) state which is the active site for ODHP reaction. For the Cr/Si catalyst, the Cr(III) state is converted into the inactive Cr(II) state within 90 s during the ODHP reaction. With increasing ODHP reaction time, the Cr(II) state increases and active sites are transformed which is equivalent to 'catalytic deactivation' in the ODHP reaction. Interestingly, for the Ni promoted catalyst, the Cr(III) state is well maintained during the catalytic reaction, indicating that the active sites are still maintained. Therefore, it can be concluded that by introducing Ni on Cr/Si catalyst, catalyst deactivation can be reduced and the regeneration of active sites can be achieved.

By combining the 3-step $H_2$-TPR and the *ex situ* XPS results, we could propose the mechanism of ODHP reaction of 0.5Ni-Cr/Si catalyst as shown in Scheme 3-1. Cr(VI) states in the $CrO_x$ are instantly reduced to Cr(III) upon interaction of propane which act as a precursor for active sites. The formed coordinatively unsaturated Cr(III) states work for dehydrogenation

and the generated hydrogen reduce Cr(III) to Cr(II) state which causes the deactivation of the catalyst. The soft oxidant $CO_2$ is activated and dissociated on the Ni surface nearby chromium oxide and the generated $O^*_{ads}$ is transferred to re-oxidize Cr(II) to Cr(III) and Cr(III) to Cr(VI) step by step to recover the original $CrO_x$ phase. Consequently, 0.5Ni-Cr/Si catalyst shows high stability in ODHP reaction by maintaining the active their Cr(III) states.

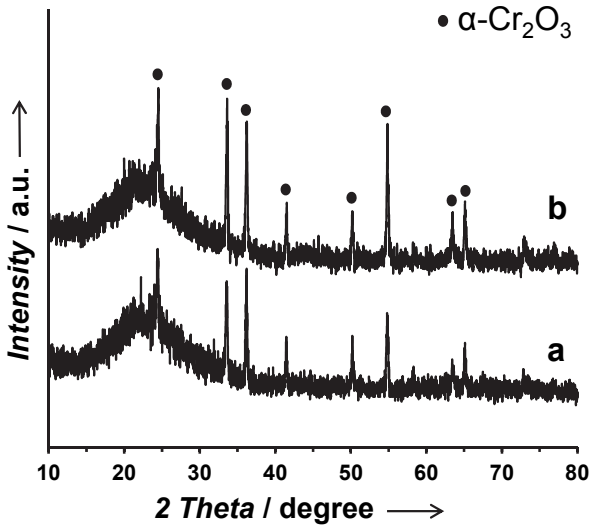


**Figure 3-1.** X-ray diffraction patterns of (a) Cr/Si and (b) 0.5Ni-Cr/Si catalysts.

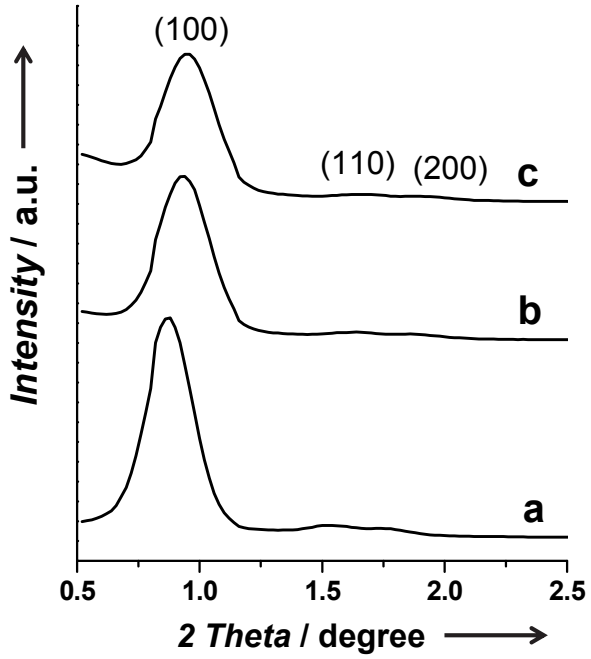


**Figure 3-2.** Small-angle X-ray diffraction patterns of (a) SBA-15, (b) Cr/Si and (c) 0.5Ni-Cr/Si.

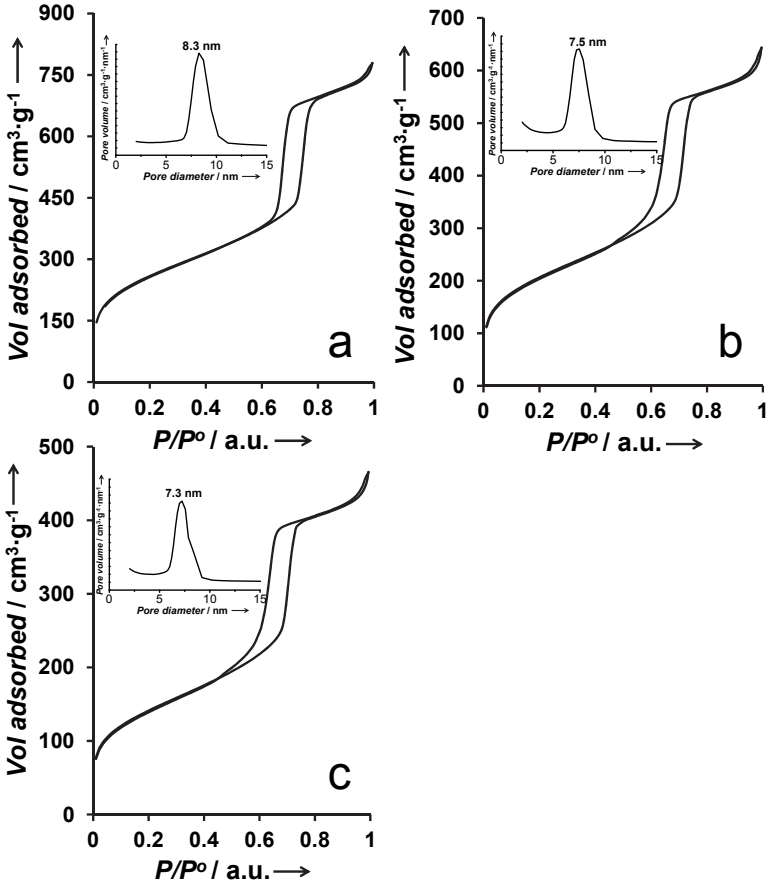


**Figure 3-3.** $N_2$ adsorption-desorption isotherms (inset: pore size distributions) of (a) SBA-15, (b) Cr/Si and (c) 0.5Ni-Cr/Si.

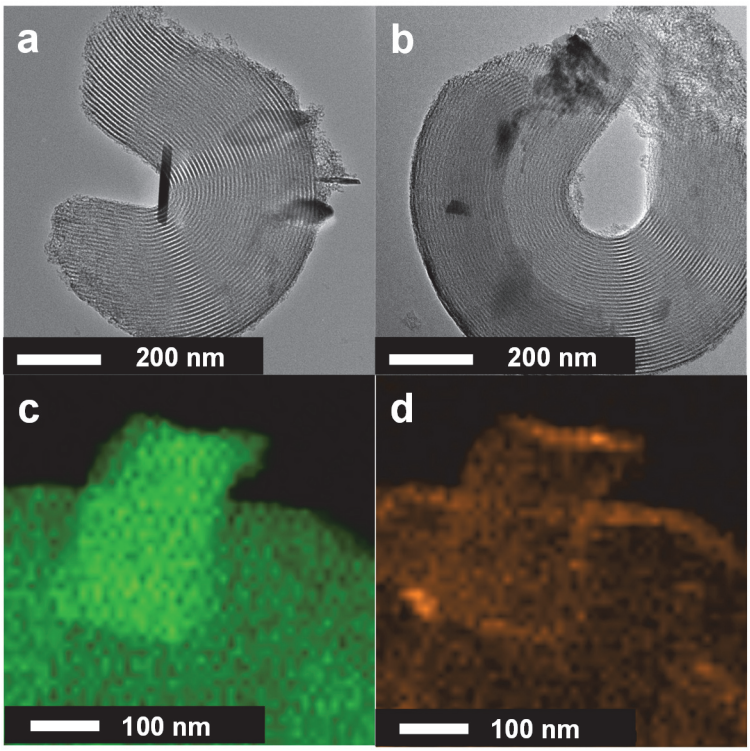


**Figure 3-4.** HR-TEM images of (a) Cr/Si and (b) 0.5Ni-Cr/Si catalysts and (c) 2-D atomic mapping by using analytical STEM equipped with EDS for Cr and Ni of the 0.5Ni-Cr/Si catalyst.

**Table 3-1.** Structural and textural parameters of catalysts.

| Catalyst | Lattice parameter [nm][a] | Surface area $[m^2 \cdot g^{-1}]$[b] | Pore volume $[cm^3 \cdot g^{-1}]$[c] | Pore size [nm][d] | Wall thickness [nm][e] |
|---|---|---|---|---|---|
| SBA-15 | 11.5 | 912 | 1.2 | 8.3 | 3.2 |
| Cr/Si | 10.9 | 732 | 1.0 | 7.5 | 3.4 |
| 0.5Ni-Cr/Si | 10.6 | 504 | 0.7 | 7.2 | 3.4 |

[a] Calculated from $d_{100}$ spacing with $a = d_{100}(2/\sqrt{3})$; [b] BET surface area; [c] BJH cumulative pore volume; [d] Pore sizes were derived from the adsorption branches of the isotherms by using the BJH method; [e] Calculated by subtraction of pore size from lattice parameter.

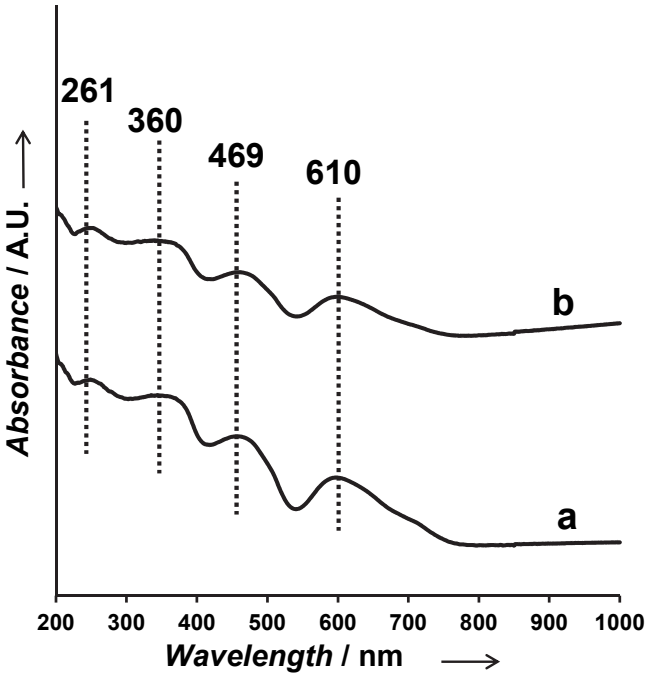


**Figure 3-5.** Diffuse reflectance UV-Vis spectra of (a) Cr/Si and (b) 0.5Ni-Cr/Si catalyst.

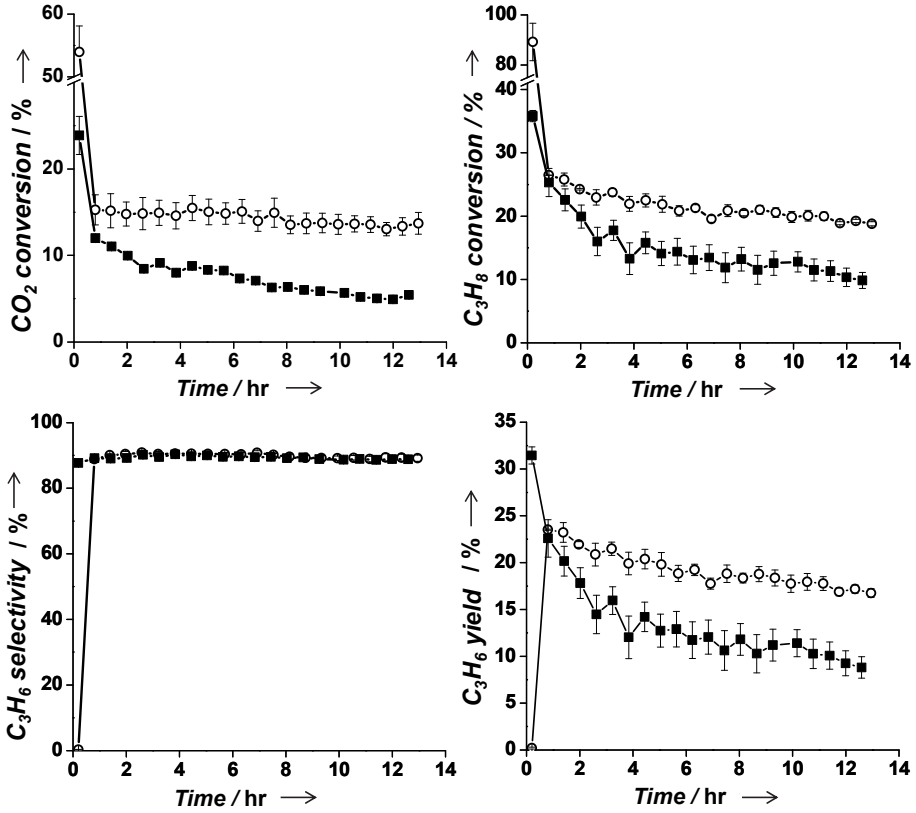


**Figure 3-6.** ODHP reaction catalytic test of the (■) Cr/Si and (○) 0.5Ni-Cr/Si catalysts.

**Table 3-2.** C weight ratio (%) evaluated by CHNS elementary analysis of Cr/Si and 0.5Ni-Cr/Si catalyst.

| Catalyst | Fresh Catalyst[a] | Used Catalyst[b] |
|---|---|---|
| Cr/Si | 0.2 | 12.2 |
| 0.5Ni-Cr/Si | 0.1 | 16.8 |

[a] As synthesized [b] after the ODHP reaction for 12 h.

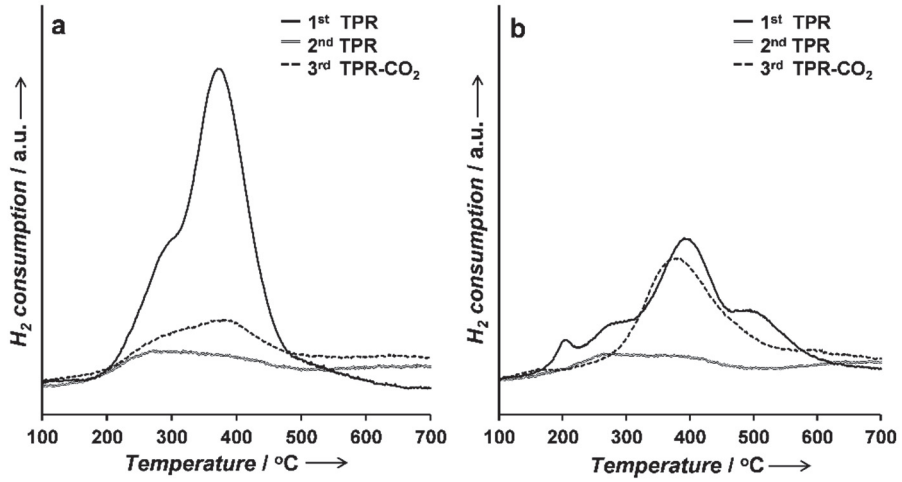


**Figure 3-7.** 3-step $H_2$-temperature programmed reduction of (a) Cr/Si and (b) 0.5Ni-Cr/Si catalyst.

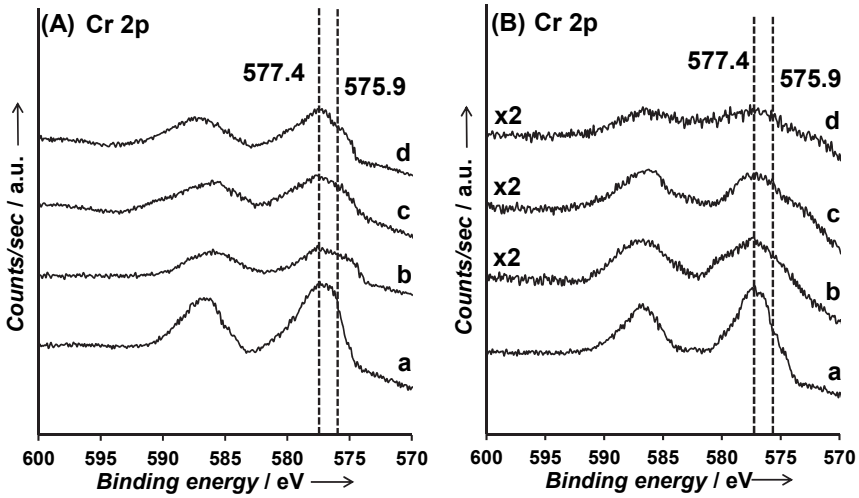


**Figure 3-8.** XPS Cr 2p region spectra of (A) Cr/Si and (B) 0.5Ni-Cr/Si catalyst: (a) before the reaction; after (b) 90 s, (c) 5 min, and (d) 12 min ODHP reaction.

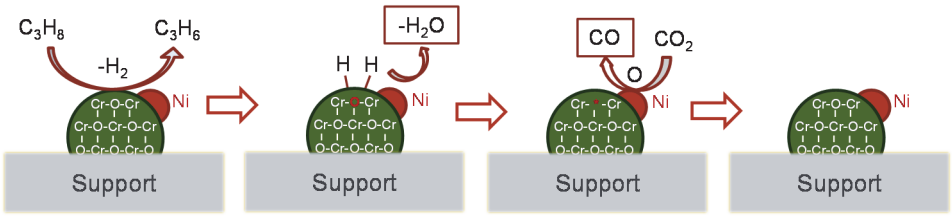


**Scheme 3-1.** Proposed mechanism of ODHP reaction of 0.5Ni-Cr/Si catalyst.

# Chapter 4. Esterification/Pyrolysis Reaction for the Production of 1,3-Butadiene from Biomass Derived 2,3-Butanediol

## 4.1 Introduction

The worldwide lack of petroleum has stimulated a search for alternative sources of clean energy. The use of biomass for this purpose, turning consumptive use into recyclable use, is an ideal goal for the future. The use of feedstock derived from biomass, e.g., sugars, vegetable oil, lignocellulosic biomass, and algae emits the greenhouse gas, carbon dioxide, but it can be reused in the photosynthetic process and could result in the creation of a carbon-neutral and sustainable society [122].

Glucose, a monosaccharide produced by plants could be efficiently utilized after a fermentation process as the carbon source for microorganisms [123]. Glucose can be converted into 2,3-butanediol by fermentation in which the major byproducts are formic acid and acetic acid (C1-C2 acids), although the proportion of these byproducts can vary, depending on the conditions of the fermentation [124]. The use of 2,3-butanediol is expected to steadily increase because its derivatives can be used in the production of synthetic rubber, plasticizers, and fuel additives. Therefore, the development of a suitable technology for the conversion of 2,3-butanediol into other

value-added products such as 1,3-butadiene would be highly desirable [125, 126]. 1,3-Butadiene is currently produced by the steam cracking of paraffinic hydrocarbons, the catalytic dehydrogenation of n-butane and n-butene, and the oxidative dehydrogenation of n-butene, all of which are based on a petrochemical process [127].

Herein, we report on a process for the production of 1,3-butadiene from the mixture of 2,3-butanediol and C1-C2 acids which are representative products in glucose fermentation. Importantly, this process can replace some petrochemical-based processes. We proved that esterification would occur between the 2,3-butanediol and C1-C2 acids to form di-esters (product **4** and **7**). In addition, the C-O cleavage in the di-ester (product **4** and **7**) sequentially proceeds during the pyrolysis process, which results in the selective formation of 1,3-butadiene (Scheme 4-1). A similar procedure was reported in 1945 by S. Marshak and co-workers, however, the experimental details concerning it are not available [128].

To the best of our knowledge, the present work is the first report of esterification followed by pyrolysis for the formation of 1,3-butadiene by reacting 2,3-butanediol with products produced by the fermentation of glucose. This process would result in diminished cost and energy which are consumed in the pre-separation of reactants including 2,3-butanediol and C1-C2 acids. In addition, 1,3-butadiene (gas phase) can be easily isolated from the glucose fermentation products.

## 4.2 Experimental

### 4.2.1 General procedure for the esterification process

A mixture of 2,3-butanediol with formic acid or acetic acid and 0.2 ml of sulfuric acid were placed in a round-bottomed flask fitted with a Dean-Stark trap and a condenser. The solution was stirred and the reaction temperature was gradually increased from 110 $^{o}$C to 130 $^{o}$C and 110 $^{o}$C to 140 $^{o}$C for the esterification of 2,3-butanediol with formic acid and acetic acid, respectively (Direct increasing of reaction temperature results in the higher yield of methyl ethyl ketone and loss of C1-C2 acids used for the esterification). The resulting mixture was then extracted with dichloromethane and the organic layer was dried over anhydrous esterification). The resulting mixture was then extracted with dichloromethane and the organic layer was dried over anhydrous magnesium sulfate, filtered, and flash evaporated. The liquid products were analyzed by GC using a Younglin YL 6100 gas chromatograph equipped with a FID. The amount of loss of C1-C2 acids during the esterification was analyzed by HPLC using Younglin YL 9100.

### 4.2.2 General procedure for the pyrolysis process

The pyrolysis in the absence of catalyst was carried out in a flow-type quartz reactor, which was then placed in an electric furnace. The temperature was monitored by means of a K-type thermocouple controlled by a PID

controller in the range of 400- 600 $^{o}$C. The feed was preheated to 250 $^{o}$C in a stream of dry $N_2$ (30 $cm^3min^{-1}$). The feed consisted of a mixture of organic phase and the flow rate was set as 0.3 $mLh^{-1}$. The liquid hourly space velocity (LHSV) was calculated from the volumetric feed rate and volume of reactor. The liquid phase after pyrolysis was trapped in 30 mL of methanol cooled at -15 $^{o}$C and analyzed using Agilent 7890 gas chromatograph coupled with a model 5975 mass spectrometer. The output gas phase stream was analyzed using an on-line gas chromatograph Donam DS 6200. For the quantification of loss of C1-C2 acids during the pyrolysis, D. I. water was used for the trapping agent produced C1-C2 acids and analyzed by HPLC using Younglin YL 9100. The coke formation was analysed by CHNS-932 elemental analyser using $SiO_2$ (Degussa, Aerosil 200) as an inert material.

### 4.2.3 Characterization of products

New compounds were characterized by $^{1}$H NMR, $^{13}$C NMR and high resolution mass spectra (HRMS). $^{1}$H and $^{13}$C NMR spectra were recorded on a Bruker Avance 500 MHz NMR spectrometer. Chemical shifts (δ) are qouted in parts per million relative to acetone-$d_6$ 2.05 ppm for $^{1}$H and 29.92 ppm for $^{13}$C as the internal standard. HRMS were measured with a JEOL JMS-700 instrument and accurate masses were reported for the molecular ion ($M^+$).

4.2.4 Electrostatic potential map of products

The electrostatic potential map was produced using the GaussView 5.0 program based on the DFT (density functional theory) calculation results. All structures were fully optimized at the DFT level using B3LYP hybrid functional and 6-311 basis set by Gaussian 03W program package. The reported optimized structure of (R,S)-2,3-butanediol was used to construct the initial structure of the formic acid 2-hydroxy-1-methyl-propyl ester (**3**) and the formic acid 2-formyloxy-1-methyl-propyl ester (**4**) [129].

## 4.3 Results and discussion

### 4.3.1 Composition of glucose fermentation products

The composition of glucose fermentation liquor by Klebsiella oxytoca KCTC12133BP (Korean Collection for Type Cultures, Daejeon, Korea) is presented in Table 4-1. The microbial fermentation experiment and the analysis was conducted by GS-Caltex Corporation. As can be seen from Table 4-1, the glucose fermentation liquor is comprised of 2,3-butanediol as the main product, followed by formic acid, acetic acid, lactic acid, succinic acid (C1-C4 acids), and acetoin, along with some inorganic salts. The molar ratio of 2,3-butanediol, formic acid, and acetic acid is typically 1 : 0.5 : 0.1 in the liquor where the amount of 2,3-butandiol is dominant. It should be noted that the isomer ratio between *meso* and *racemic* 2,3-butanediol used for the esterification coincide with the that of glucose fermentation product (*meso* : *racemic* = 9 : 1).

The esterification process was evaluated as the first step using sulfuric acid as a catalyst. After the reaction, the sulfuric acid can be recovered in the course of the extraction procedure. The stoichiometric molar ratio between 2,3-butanediol and C1-C2 acids is 1:2, as shown in Scheme 4-1. However, taking the relatively low boiling point of formic acid (100.8 $^{o}$C) and acetic acid (118 $^{o}$C) into account, excess C1-C2 acids were used in the esterification; 2,3-butanediol (**1**) : formic acid (**2**) = 1 : 4 and 2,3-butanediol

(**1**) : acetic acid (**5**) = 1 : 2.5 molar ratio. To force the equilibrium to the right, a Dean-Stark trap was used to remove water from the reaction mixture.

### 4.3.2 Esterification of 2,3-butanediol with formic acid

The esterification between 2,3-butanediol (**1**) and formic acid (**2**) occurs sequentially, in which the formic acid 2-hydroxy-1-methyl-propyl ester (**3**) is formed first and another 2,3-butanediol (**1**) reacts with product **3** to produce formic acid 2-formyloxy-1-methyl-propyl ester (**4**) (Scheme 4-2). This reaction process can be confirmed by time-on-stream reaction experiments (Figure 4-1) as the continuous decrease in formic acid 2-hydroxy-1-methyl-propyl ester (**3**) is correlated with the gradual increase of 2,3-butanediol (**1**) conversion and formic acid 2-formyloxy-1-methyl-propyl ester (**4**) formation until 7 h of reaction time. The desired product formic acid 2-formyloxy-1-methyl-propyl ester (**4**) for 1,3-butadiene was obtained with 70 % selectivity as well as formic acid 2-hydroxy-1-methyl-propyl ester (**3**) with 17% selectivity as an intermediate within 5 h at 130 $^{o}$C (Figure 4-1). The calculated m/z for the formic acid 2-formyloxy-1-methyl-propyl ester (**4**) was 147.0657 and measured as 147.0659 and the structure was additionally confirmed by $^{1}$H NMR and $^{13}$C NMR. As the reaction proceeded, the color of the reaction mixture changed from light yellow to light brown. This color change can be attributed to the increased production of formic acid 2-formyloxy-1-methyl-propyl ester (**4**). While the composition of formic acid 2-hydroxy-1-methyl-propyl ester (**3**) and unknown products changed during

the course of the reaction of 5 h to 7 h, the yield of the targeted formic acid 2-formyloxy-1-methyl-propyl ester (**4**) was maintained at a constant level of 70%, indicating that the formation and degradation rates of formic acid 2-formyloxy-1-methyl-propyl ester (**4**) are equal. After 7 h of reaction time, however, the yield of other compounds originating from 2-formyloxy-1-methyl-propyl ester (**4**) rapidly increased as the decreased amount of product **4** was transformed into other products. Hence, the optimum time for the esterification between 2,3-butanediol and formic acid was 5 h at 130 $^{o}$C. After the reaction, the loss of excess formic acid was calculated to be 2%. For the subsequent experimental pyrolysis process, we used an esterification mixture that was produced after a reaction time of 5 h.

### 4.3.3 Esterification of 2,3-butanediol with acetic acid

We further investigated the esterification of 2,3-butanediol (**1**) with acetic acid (**5**) (Scheme 4-3). The esterification products resulted in the formation of the corresponding acetic acid 2-hydroxy-1-methyl-propyl ester (**6**) and acetic acid 2-acetoxy-1-methyl-propyl ester (**7**); the chemical structures of which were confirmed from $^{1}$H-NMR and $^{13}$C NMR data. Also, the m/z estimated for the acetic acid 2-acetoxy-1-methyl-propyl ester (**7**) was 175.0970 and the measured value was 175.0971. An evaluation of esterification using 2,3-butandeiol with acetic acid time-on-stream (Figure 4-2) indicates that the optimum time required for the reaction is 10 h where the selectivity of acetic acid 2-acetoxy-1-methyl-propyl ester (**7**) is enhanced at

the expense of acetic acid 2-hydroxy-1-methyl-propyl ester (**6**) as the reaction proceeded. After 10 h, reaction mixture turned dark brown which can be attributed to the production of acetic acid 2-acetoxy-1-methyl-propyl ester (**7**). Unlike the esterification of 2,3-butanediol with formic acid, the formed acetic acid 2-acetoxy-1-methyl-propyl ester (**7**) was not degraded into other products. The esterification of 2,3-butanediol with acetic acid required an extended reaction time to achieve the maximum production of acetic acid 2-acetoxy-1-methyl-propyl ester (**7**) compared to the esterification of 2,3-butanediol with formic acid; this can be attributed to the steric effect conferred by the longer alkyl chain [130]. It should be noted, however, that the selectivity at the equilibrium state for acetic acid 2-acetoxy-1-methyl-propyl ester (**7**) (selectivity: 85%) is higher than formic acid 2-formyloxy-1-methyl-propyl ester (**4**) (selectivity: 70%), indicating that the selectivity in the reaction is influenced more by thermodynamics than the steric hindrance caused by length of the alkyl chain. In this experiment, no loss of acetic acid was observed. The esterification mixture production after a reaction time of 10 h was used in the subsequent pyrolysis step.

### 4.3.4 Pyrolysis of esterificated products

Considering the proposed mechanism shown in Scheme 4-1, the pyrolysis of formic acid 2-formyloxy-1-methyl-propyl ester (**4**) and acetic acid 2-acetoxy-1-methyl-propyl ester (**7**) would sequentially occur following the

esterification reaction to produce 1,3-butadien. In this step, the pyrolysis of formic acid 2-formyloxy-1-methyl-propyl ester (**4**) and acetic acid 2-acetoxy-1-methyl-propyl ester (**7**) would proceed in the absence of a catalyst at a relatively high temperature.

Electrostatic potential maps for the formic acid 2-hydroxy-1- methyl-propyl ester (**3**) and formic acid 2-formyloxy-1-methyl-propyl ester (**4**) show that the electron densities are highly localized on ester groups, which can function as a good leaving group because the anion produced in the reaction is stable (Figure 4-3, we only discuss product **3** and **4** as a similar explanation can be valid for product **6** and **7**). In the case of product **3**, since the –OH in 2,3-butanediol is a much poorer leaving group; it is typically aided by protonation, the electrophilic ester functional group leaves first via cleavage of the C-O bond to give a secondary carbocation [131]. Consistent with the E1 mechanism in organic chemistry, the ester anion would attack the β-hydrogen in the carbocation intermediate with the regeneration of formic acid and the production of a carbon-carbon double bond in the carbocation intermediate.[11] This step is repeated in another ester functional group in product **4** with 1,3-butadiene being produced as a final product. When the elimination of the ester functional group occurs in the mono-ester (product **3** and **6**), 3-buten-2-ol and methyl ethyl ketone are readily produced. The formation of the carbocation intermediate crosses the high energy barrier which is the rate-determining step in the reaction, and, because of this, a high temperature is required for the pyrolysis of formic acid 2-formyloxy-1-

methyl-propyl ester (**4**) and acetic acid 2-acetoxy-1- methyl-propyl ester (**7**) [132].

The reaction temperature in the pyrolysis was optimized in the range of 400-600 $^{o}$C (Figure 5-4a). In the early of pyrolysis, the yield of 1,3-butadiene was lowered due to the slightly soluble property of 1,3-butadiene in the methanol [133]. The constant yield of 1,3-butadiene could be obtained after 5 h. When the reaction occurred at 400 $^{o}$C, the conversion of acetic acid 2-acetoxy-1-methyl-propyl ester (**7**) was lowered. An increase in the reaction temperature to 600 $^{o}$C, however, promoted the decomposition of the products, resulting in the formation of C1-C3 hydrocarbons (methane, ethylene, and propylene). Based on the above results, the reaction temperature for the pyrolysis was set at 500 $^{o}$C for the conversion of all of the esterification products with high selectivity for 1,3-butadiene. In the pyrolysis of formic acid 2-formyloxy-1-methyl-propyl ester (**4**), the selectivity was about 94 % whereas it was 82% for acetic acid 2-acetoxy-1-methyl-propyl ester (**7**) (Figure 4-4b). The high selectivity for 1,3-butadiene in the pyrolysis can be attributed to the selective elimination of the ester functional group as explained in Figure 4-3. It is noteworthy that coke formation after the pyrolysis step is negligible (0.5% for the pyrolysis of product **7**). In addition, an analysis of the output gas phase stream shows that highly pure 1,3-butadiene is produced. The high purity of 1,3-butadiene (the peak at 51 min in the GC chromatogram) above 93% for both the pyrolysis of formic acid 2-formyloxy-1-methyl-propyl ester (**4**) and acetic acid 2-acetoxy-1-methyl-propyl ester (**7**) were analyzed by on-line GC-FID. The small peak in the GC

chromatogram at 27 min corresponds to trans-2-butene which is the main side reaction product in gas phase along with the minor decomposition to C1-C3 hydrocarbons (methane, ethylene, and propylene). Building upon these results, this approach would be potentially useful for extracting pure 1,3-butadiene in the form of a gas phase from the glucose-derived fermentation products.

### 4.3.5 Sustainable production of 1,3-butadiene from glucose fermentation products

The attractive point of this process is that the original C1-C2 acids in the final liquid products can be recovered. If a recycling process were possible; the C1-C2 acids produced in the reaction could be transferred to the esterification process, which would permit the C1-C2 acids to accumulate where excessive amounts are needed to adjust the stoichiometric molar ratio. Given the fact that the C1-C2 acids are collected at the final stage, they could be trapped in methanol and the results were as expected. In the GC-MS chromatogram of the trapped liquid phase, formic acid and acetic acid were regenerated with methyl ethyl ketone (Figure 4-5). The recovery rate of C1-C2 acids after pyrolysis was also quantified. Interestingly, the recovery of acetic acid was 100% whereas the formic acid show the much lower recovery rate (20%) which could be related with the low stability of formic acid at high temperature [134]. Some unknown products were present in the resulting liquid phase after the pyrolysis of the esterification product using 2,3-butanediol with acetic acid. This is in agreement with the observed

decreased selectivity for 1,3- butadiene in the output gas phase stream at these conditions (Figure 4-4b).

Based on these results, we attempted to apply the model mixture to the esterification followed by pyrolysis reaction. The model mixture is proposed where it is comprised of 2,3-butanediol : formic acid : acetic acid = 1 : 0.5 : 2.5 molar ratio with considering the recovery rate of C1-C2 acids throughout the two sequential reactions and low boiling point of C1-C2 acids. This model mixture proportion allows the process to be recycled if an additional 2.4 mol of acetic acid is added to the glucose fermentation liquor (2,3-butanediol : formic acid : acetic acid = 1 : 0.5 : 0.1). The reaction temperature was increased to 140 $^{o}$C in the light of dominant composition of acetic acid in the model mixture. In Table 4-2, conversion of 2,3-butanediol showed 100% after 3 h which can be attributed to enough amounts of C1-C2 acids for the esterification reaction step. In accordance with the previous esterification results, the composition of mono-esters (product **3** and **6**) decreased as the reaction proceeded by the self-destruction to the di-esters (product **4** and **7**). The produced product **4** and **7** are also confirmed. Interestingly, entirely new peak in the GC-FID chromatogram was generated and it is confirmed as acetic acid 2-formyloxy-1-methyl-propyl ester (**8**) where each formic acid and acetic acid comprise two ester functional group to one 2,3-butanediol molecule. The product **8** also has capability of producing 1,3-butadiene with a high selectivity of 92% (data not shown here). It should be noted that the yield of di-esters (product **4**, **7**, and **8**) remained essentially unchanged after a reaction time of 10 h. Thus, the optimum

reaction time is considered to be 10 h for the following pyrolysis. Concerning the origin of 1,3-butadiene, one can predict the yield of 1,3-butadiene from the glucose fermentation is maximized at 83%. Finally, 70% of the 1,3-butadiene was obtained via the pyrolysis reaction after 5 h (Table 4-3). This is probably the highest yield ever reported [135]. Along with the obtained high yield of 1,3-butadiene from glucose fermentation liquor, the recycling of recovered C1-C2 acids after pyrolysis as reactants has considerable merit from the environmental and economic point of view.

### 4.3.6 Another strategy for the production of 1,3-butadiene from 2,3-butanediol

To verify the usefulness of dehydrative epoxidation, we suggest a catalytic process for the production of 1,3-butadiene from 2,3-butanediol (meso-BD) (Scheme 4-4). To the best of our knowledge, this catalytic process is the first reported where the entire process is comprised of heterogeneous catalytic system. The trans-epoxibutane (trans-EB) formed via the dehydrative epoxidation of meso-BD is sufficiently reactive to be further dehydrated to 1,3-butadiene. However, the dehydration of epoxybutane over an acid catalyst (Al-MCM-41) did not result in the selective formation of 1,3-butadiene (yield: 19%). In order to resolve the problem, the isomerization of epoxybutane into 3-butene-2-ol (BO) needs to take place prior to the subsequent dehydration as the reaction of 3-butene-2-ol (BO) results in the selective production of 1,3-butadiene (yield: 97%). The isomerization in this

reaction was effectively induced by the bifunctional lithium phosphate ($Li_3PO_4$) which was previously utilized in the isomerization of propylene oxide. Both the *cis*-epoxibutane and *trans*-EB were selectively converted to BO, but the use of *trans*-EB resulted in a more selective reaction (92, 75% for *trans*-EB and *cis*-EB, respectively). On the basis of these results, highly selective production of 1,3-butadiene (~75% selectivity) can be achieved from biomass derived 2,3-butanediol.

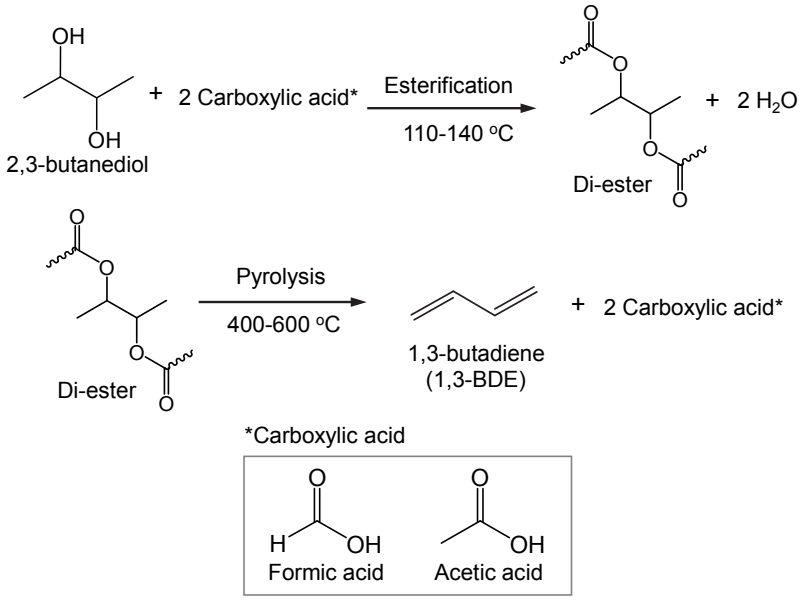


**Scheme 4-1.** Conversion of biomass-derived 2,3-butanediol and carboxylic acid to 1,3-butadiene.

**Table 4-1.** Composition of microbial fermented liquor.

(Unit: g/kg)

| 2,3-butanediol | Formic acid | Acetic acid | Acetoin | Lactic acid | Succinic acid | Ethanol |
|---|---|---|---|---|---|---|
| 480.13 | 122.64 | 13.91 | 5.08 | 34.10 | 36.93 | 0.00 |

(Unit: ppm (w))

| $Cl^-$ | $PO_4^{3-}$ | $SO_4^{2-}$ | $Na^+$ | $NH_4^+$ | $K^+$ | $Mg^{2+}$ | $Ca^{2+}$ |
|---|---|---|---|---|---|---|---|
| 2,850 | 70,962 | 48,760 | n.a. | n.a. | n.a. | n.a. | n.a. |

[a] See the reference for the detailed information concerning the microbial fermentation of glucose using Klebsiella oxytoca KCTC12133BP (Korean Collection for Type Cultures, Daejeon, Korea) [136].

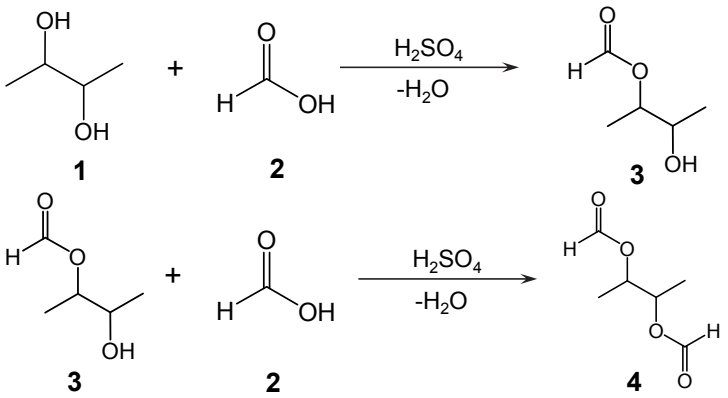


**Scheme 4-2.** Esterification of 2,3-butanediol (**1)** with formic acid (**2)** using sulfuric acid.

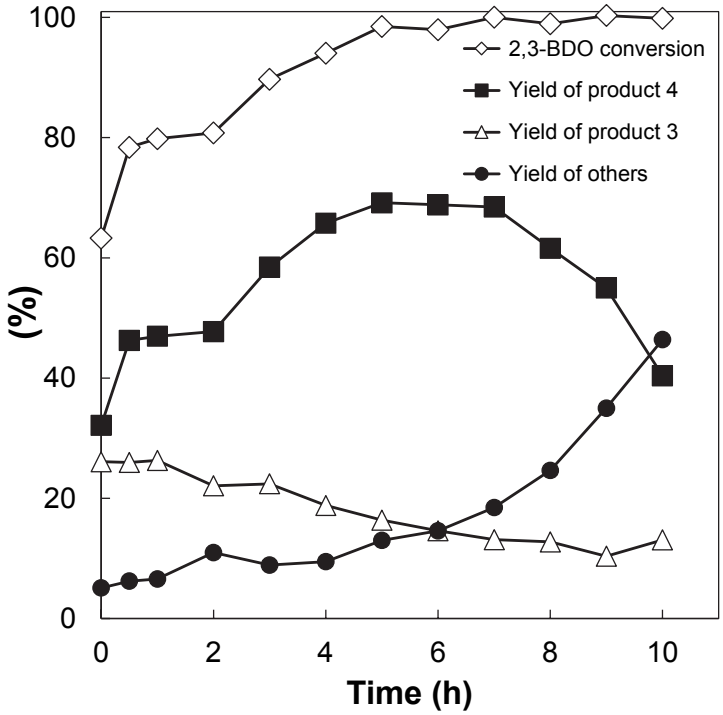


**Figure 4-1.** Time-on-stream of esterification of 2,3-butanediol with formic acid. Reaction conditions: **1** (0.22 mol), **2** (0.88 mol) and 0.2 mL of $H_2SO_4$. The temperature of the reaction mixture gradually increased during the course of the run from about 110 °C to 130 °C. The conversion of 2,3-butanediol and selectivity was determined by GC-FID.

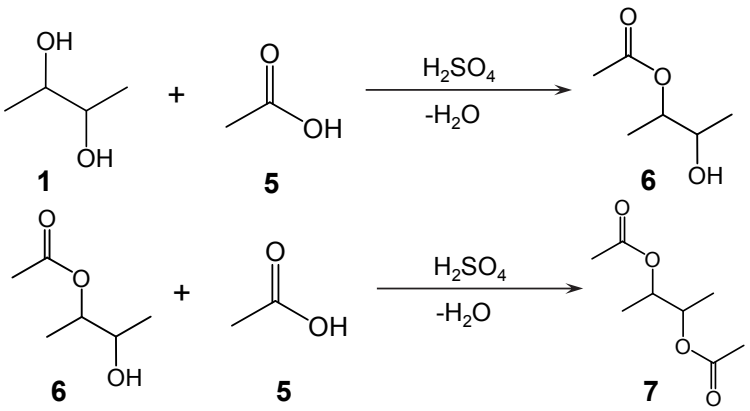


**Scheme 4-3.** Esterification of 2,3-butanediol (**1)** with acetic acid (**5)** using sulfuric acid.

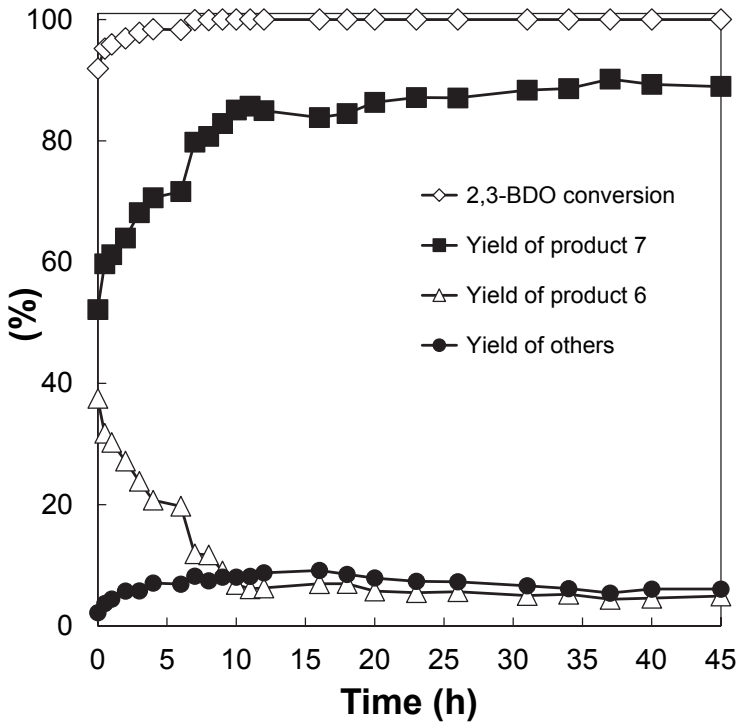


**Figure 4-2.** Time-on-stream of esterification of 2,3-butanediol with acetic acid. Reaction conditions: **1** (0.22 mol), **5** (0.55 mol) and 0.2 mL of $H_2SO_4$. The temperature of the reaction mixture gradually increased during the course of the run from about 110 $^oC$ to 140 $^oC$. The conversion of 2,3-butanediol and selectivity was determined by GC-FID.

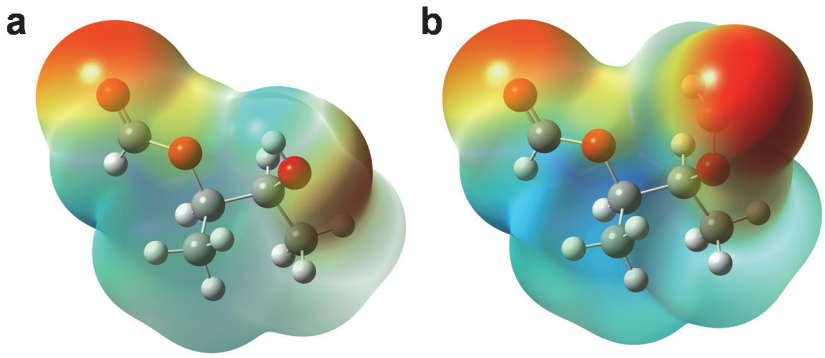


**Figure 4-3.** Electrostatic potential map for (a) formic acid 2-hydroxy-1-methyl-propyl ester (**3**) and (b) formic acid 2-formyloxy-1-methyl-propyl ester (**4**).

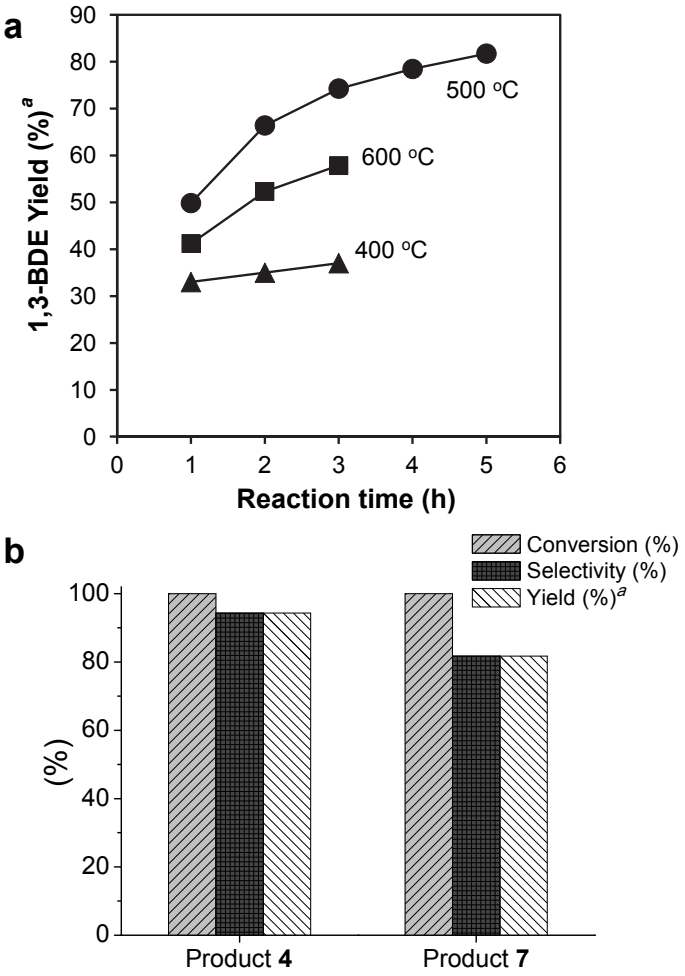


**Figure 4-4.** (a) Pyrolysis results for product **7** at 400 °C, 500 °C, and 600 °C; (b) Pyrolysis result of product **4** and **7** after 5 h at 500 °C in the absence of catalyst. Reaction conditions: 0.3 $cm^3$ $h^{-1}$ of feed flow rate, 30 $cm^3$ $min^{-1}$ of $N_2$, LHSV = 0.028 $h^{-1}$. The final liquid products were trapped in methanol. [a] Yield (%) = produced 1,3-butadiene (mol) compared to introduced product **4** (mol) and **7** (mol).

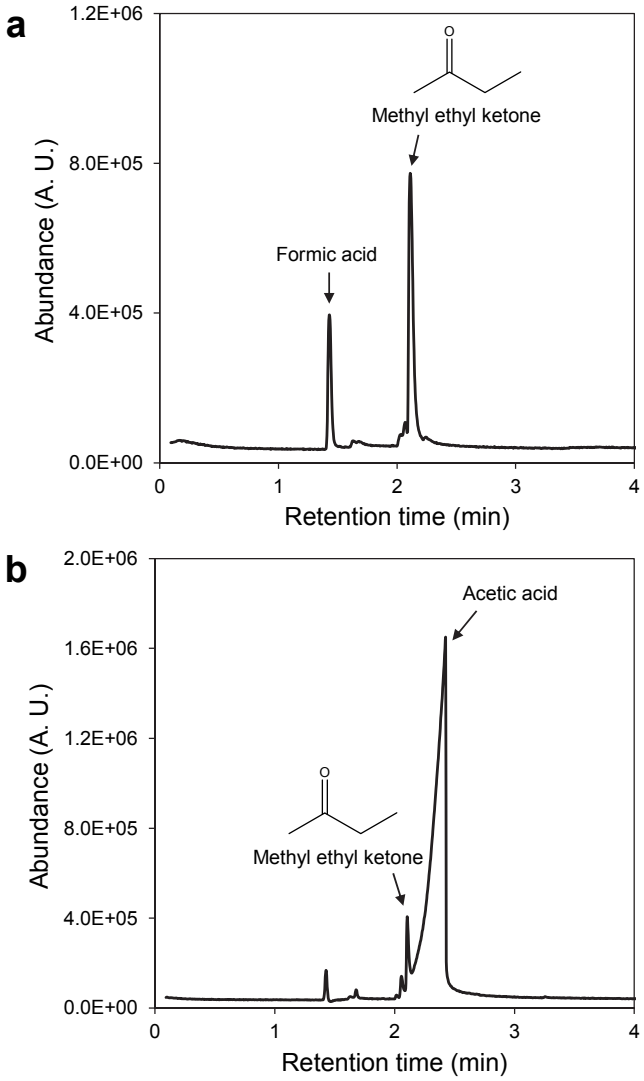


**Figure 4-5.** GC-MS chromatogram of the liquid products obtained after the pyrolysis of (a) product **4** and (b) **7** (500 $^{o}$C, 5 h, the final liquid products were trapped in methanol).

**Table 4-2.** Esterification of model mixture glucose fermentation liquor[a]

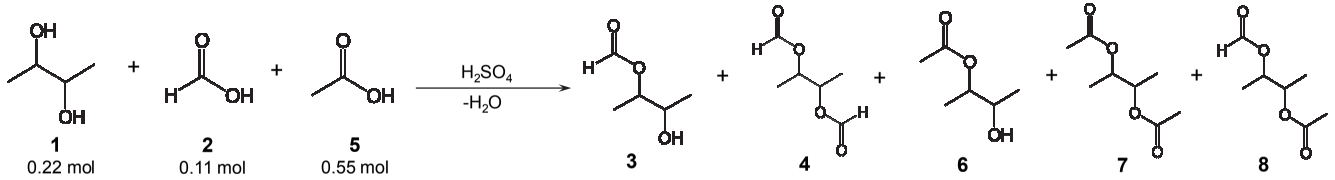


| Entry | Temperature (°C) | Time (h) | Conversion (%) | Selectivity in organic phase (%)[b] | | | | | |
|---|---|---|---|---|---|---|---|---|---|
| | | | | **3** | **4** | **6** | **7** | **8** | others |
| 1 | 140 | 3 | 99 | 3 | 2 | 17 | 54 | 18 | 6 |
| 2 | 140 | 7 | 100 | 2 | 1 | 11 | 60 | 18 | 8 |
| 3 | 140 | 10 | 100 | 1 | 1 | 7 | 66 | 16 | 9 |
| 4 | 140 | 12 | 100 | 1 | 1 | 7 | 68 | 15 | 8 |

[a] Reaction conditions: **1** (0.22 mol), **2** (0.11 mol), **5** (0.55 mol) and 0.2 mL of $H_2SO_4$. The temperature of the reaction mixture gradually increased during the course of the run from about 110 °C to 140 °C. [b] The conversion and selectivity was determined by GC-FID.

**Table 4-3.** 1,3-butadiene production from the model mixture of glucose fermentation liquor[a]

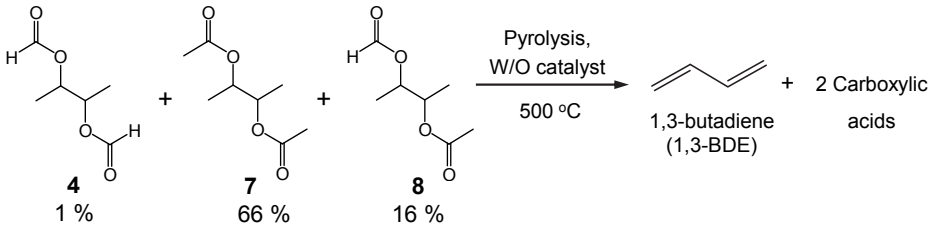


| Temperature (°C) | Time (h) | Conversion (%) | Yield (%) |
|---|---|---|---|
| 500 | 5 | 100 | 70 |

[a] Reaction conditions: The feed (Table 5-2, entry 3) flow rate was set to 0.3 $mLh^{-1}$ with 30 $cm^3$ $min^{-1}$of $N_2$ gas. LHSV = 0.028 $h^{-1}$. [b] Yield (%) = produced 1,3-butadiene relative to the initial 2,3-butanediol.

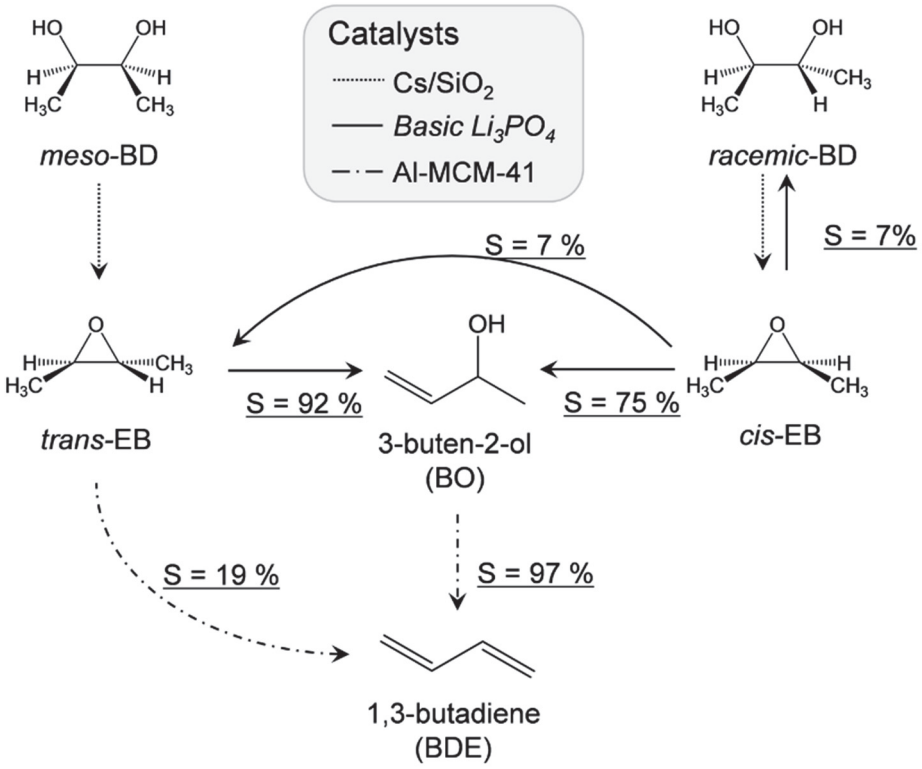


**Scheme 4-4.** Proposed catalytic process for the production of 1,3-butadiene from 2,3-butanediol.

# Chapter 5. Summary and Conclusions

It was successfully suggested a method for the synthesis of highly dispersed chromium oxide catalysts supported on MSU-x (Cr-MSU-x) and demonstrated the high catalytic activity of these materials for the oxidative dehydrogenation of propane using $CO_2$. This synthesized Cr-MSU-x catalysts showed superior catalytic activity compared to a $CrO_x$/MSU-x catalyst prepared by conventional incipient wetness impregnation which can be attributed to the fact that the chromium oxide is more highly dispersed on the MSU-x support in Cr-MSU-x catalysts. As the amount of chromium increases, the Cr-MSU-x catalysts contained various chromium species (isolated, dimers, polymeric species, and crystalline $\alpha$-$Cr_2O_3$) which can be attributed to a polymerization phenomenon. In the $H_2$-TPR characterization, we were able to classify Cr(VI) into isolated Cr(VI) and polymeric Cr(VI) species, which were designated as hard Cr(VI) and soft Cr(VI), respectively. Moreover, the initial composition of soft Cr(VI) in Cr-MSU-x catalysts mainly affected ODHP catalytic activity. This suggests that coordinatively unsaturated Cr(III) formed during the reduction of soft Cr(VI) is more active than the reduced from of hard Cr(VI). The high activity of coordinatively unsaturated Cr(III) that originated from soft Cr(VI) can be rationalized by the fact that this type of chromium species promotes the reverse RWGS reaction and undergoes a more effective redox process during the ODHP reaction as well.

Moreover, it was introduced Ni as a promoter into a 10 wt.% $CrO_x$ catalyst

supported on SBA-15 (Cr/Si) by a sequential impregnation method for use in the oxidative dehydrogenation of propane using $CO_2$ (ODHP). The crystalline form of α-$Cr_2O_3$ was not significantly affected by the added Ni but a small change; a form of nickel chromate, was confirmed by UV-Vis DRS and the 1$^{st}$ TPR peak. The synthesized NiO was easily reduced to elemental Ni, which plays the role of activating $CO_2$ to permit its dissociation to CO and activated O ($O^*_{ads}$) under the ODHP catalytic reaction conditions. In terms of catalytic activity, the addition of 0.5 wt.% Ni to the 10 wt.% Cr/Si (0.5Ni-Cr/Si) catalyst resulted in a higher $CO_2$ conversion and the stable production of propylene. The oxidizing ability of $CO_2$ was confirmed by the 3 step-TPR analysis and most of the Cr(III) state, which is the active site for the ODHP reaction, was regenerated in 0.5Ni-Cr/Si catalyst. In *ex situ* XPS measurements, the non-promoted catalyst showed a rapid transformation of active sites; reduction of the active Cr(III) to inactive Cr(II) whereas Ni allowed the catalyst to be maintained in the Cr(III) state which is enabled by the $O^*_{ads}$ generated near the Ni. This allows one to conclude that Ni has superior ability to dissociate $CO_2$ as well as to regenerate the active site in $CrO_x$ for the ODHP reaction which results in the stable yield of propylene.

Finally, an integrated route consisting of esterification followed by pyrolysis for the conversion of glucose fermentation products into 1,3-butadiene was demonstrated. This biomass-based process appears to be quite efficient, sustainable, and reusable compared with typical petrochemical processes. The catalytic esterification of 2,3-butanediol with the excess C1-C2 acids that are produced from glucose fermentation was achieved, with a 70%

and 85% selectivity for the di-ester (product **4** and **7**, respectively) in an organic phase at a 100% conversion of 2,3-butanediol. The subsequent elimination of ester functional group in the pyrolysis process enables C-O bond cleavage to occur, via E1 mechanism resulting in the formation of 1,3-butadiene and the regeneration of the C1-C2 acids. Furthermore, this combined process proceeded in the when a model mixture of glucose fermentation products were used. The present methodology provides an example of producing a diene product (1,3-butadiene) from a diol compound (2,3-butanediol) from biomass products via fermentation. Consequently, as the controlled C-O cleavage is a very general issue in the conversion of biomass-derived substrate, the procedure reported herein would be expected to have broad applicability for the production of dienes from corresponding diol compounds.

# Chapter 6. Recommendations for Further Research

The recommendations for further research are summarized as follows;

1) The investigation of substitutional catalyst with high activity for the production of propylene should be conducted for its practical usage. In spite of high activity of chromium oxide catalyst supported on mesoporous silica in ODHP reaction, it is one of items on the contraband list due to its toxicity. This impedes the introduction of technology into the petrochemical based companies where they make a new leap forward non-petrochemical based production of valuable chemicals. The research for the development of environmentally benign and better redox catalyst should be proceeded.
2) In the ODHP reaction and pyrolysis step for the production of 1,3-butadiene, they required as much as 500 - 600 $^{o}$C reaction temperature to be taken place. Such high operating temperature accompanies some side effects. As enormous thermal energy should be introduced, it arises low energy efficiency. In addition, high operating temperature inevitably involves low stability of catalyst and low selectivity for the desired product. To solve these elemental problems in catalytic reactions, therefore, development of efficient catalytic system with regard to low reaction temperature is highly suggested.

# Bibliography


[1] H. M. T. Galvis, K. P. de Jong, *ACS Catal*. **2013**, 3, 2130-2149.

[2] Wm. C. White, *Chem-Biol. Interact*. **2007**, 166, 10-14.

[3] Propylene and 1,3-butadiene with corresponding derivatives are adapted from Chiyoda Corporation database; [https://www.chiyoda-corp.com/technology/en/chemistry/c4c5.html].

[4] X. Meng, C. Xu, L. Li, J. Gao, *Energy Fuels* **2011**, 25, 1357-1363.

[5] P. Lanzafame, G. Centi, S. Perathoner, *Chem. Soc. Rev*. **2014**, 43, 7562-7580.

[6] T. Ren, M. Patel, K. Blok, *Energy* **2006**, 425-451.

[7] Y. Y. Yoshimura, N. Kijima, T. Hayakawa, K.Murata, K. Suzuki, F. Mizukami, K. Matano, T. Konishi, T. Oikawa, M. Saito, T. Shiojima, K. Shiozawa, K. Wakui, G. Sawada, K. Sato, S. Matsuo and N. Yamaoka, *Catal. Surv. Jpn*. **2000**, 4, 157-167.

[8] N. Rahimi, R. Karimzadeh, *Appl. Catal. A* **2011**, 398, 1-17.

[9] A. Corma, F. V. Melo, L. Sauvanaud, F. J. Ortega, *Appl. Catal. A* **2004**, 265, 195-206.

[10] A. Corma, F. V. Melo, L. Sauvanaud, F. J. Ortega, *Catal. Today* **2005**, 107-108, 699-706.

[11] G. Wang, C. Xu, J. Gao, *Fuel Process. Technolo*. **2008**, 89, 864-873.

[12] S. M. Sadrameli, A. E. S. Green, *J. Anal. Appl. Pyrolysis* **2005**, 73, 305-313.

[13] V. V. Krishnan, S. L. Suib, *J. Catal*. **1999**, 184, 305-315.

[14] H. Lee, J. C. Jung, H. Kim, Y.-M. Chung, T. J. Kim, S. J. Lee, S.-H. Oh, Y. S. Kim, I. K. Song, *Catal. Lett.* **2008**, 124, 364-368.

[15] J. C. Jung, H. Lee, H. Kim, Y. –M. Chung, T. J. Kim, S. J. Lee, S.-H. Oh, Y. S. Kim, I. K. Song, *J. Mo. Catal. A: Chem*. **2007**,271, 261-265.

[16] W. Yan, Q. Y. Kouk, J, Luo, Y. Liu, A. Borgna, *Catal. Commun*. **2014**, 46, 208-212.

[17] C. Wan, D.-G. Cheng, F. Chen, S. Zhan, *Chem. Eng. Sci*. **2014**, http://dx.doi.org/10.1016/j.ces.2014.08.020.

[18] J.-H. Park, K. Row, C.-H. Shin, *Catal. Commun*. **2013**, 31, 76-80.

[19] S. Furukawa, M. Endo, T. Komatsu, *ACS Catal*. **2014**, 4, 3533-3542.

[20] Y. Ren, F. Zhang, W. Hua, Y. Yue, Z. Gao, *Catal. Today* **2009**, 148, 316-322.

[21] M. Chen, J. Xu, Y. M. Liu, Y. Cao, H. Y. He, J. H. Zhuang, *Appl. Catal. A* **2010**, 377, 35-41.

[22] L. Liu, H. Li, Y. Zhang, *Catal. Commun.* **2007**, 8, 565-570.

[23] B. Schimmoeller, Y. Jiang, S. E. Pratsinis, A. Baiker, *J. Catal.* **2010**, 274, 64-75.

[24] P. Michorczyk, J. Ogonowski, *React. Kinet. Catal. Lett.* **2003**, 78, 41-47.

[25] M. Salmanca, Y. E. Licea, A. Echavarria, A. C. Faro Jr, L. A. Palacio, *Phys. Chem. Chem. Phys.* **2009**, 11, 9583-9591.

[26] Y. M. Liu, Y. Cao, S. R. Yan, W. L. Dai, K. N. Fan, *Catal. Lett.* **2003**, 88, 61-67.

[27] J. S. Gonzálẹz, J. M. Robles, M. A. Rodríguez, P. M. Torres, E. R. Castellón, A. J. López, *Catal. Lett.* **2000**, 64, 209-214.

[28] F. Cavani, R. Trifiro, *Catal. Today* **1995**, 24, 307-313.

[29] *Ž*. S. Kotanjac, M. V. S. Annaland, J. A. M. Kuipers, *Chem. Eng. Sci.* **2010**, 65, 441-445.

[30] T. Davies, S. H. Taylor, *Catal. Lett.* **2004**, 93, 151-154.

[31] K. Takehira, Y. Ohishi, T. Shishido, T. Kawabata, K. Takaki, Q. Zhang, Y. Wang, *J. Catal.* **2004**, 224, 404-416.

[32] Y. Sakurai, T. Suzaki, N. Ikenaga, T. Suzuki, *Appl. Catal. A* **2000**, 192, 281-288.

[33] H. Y. Li, Y. Yue, C. Miao, Z. Xie, W. Hua, Z. Gao, *Catal. Commun.* **2007**, 8, 1317-1322.

[34] S. Wang, Z. H. Zhu, *Energy Fuels* **2004**, 18, 1126-1139.

[35] J. S. Chang, V. P. Vislovskiy, M. S. Park, D. Y. Hong, J. S. Yoo, S. E. Park, *Green Chem.* **2003***,* 5, 587-590.

[36] S. Wang, K. Murata, T. Hayakawa, S. Hamakawa, K. Suzuki, *Appl. Catal. A* **2000**, 196, 1-8.

[37] P. Michorczyk, J. Ogonowski, *Appl. Catal. A* **2003**, 251, 425-433.

[38] W. Daniell, A. Ponchel, S. Kuba, F. Anderle, T. Weingand, D. H. Gregory, H. Knözinger, *Top. Catal.* **2002**, 20, 65-74.

[39] E. V. Kondratenko, A. Brückner, *J. Catal.* **2010**, 274, 111-116.

[40] I. Takahara, W. C. Chang, N. Mimura, M. Saito, *Catal. Today* **1998**, 45, 55-59.

[41] E. Rombi, M. G. Cutrufello, V. Solinas, S. D. Rossi, G. Ferraris, A. Pistone, *Appl. Catal. A* **2003**, 251, 255-266.

[42] M. Cherian, M. S. Rao, A. M. Hirt, I. E. Wachs, G. Deo, *J. Catal.* **2002**, 211, 482-495.

[43] L. C. Liu, H. Q. Li, Y. Zhang, *Kinet. Catal.* **2009**, 50, 684-690.

[44] T. V. M. Rao, E. M. Zahidi, A. Sayari, *J. Mol. Catal. A: Chem.* **2009**, 301, 159-165.

[45] S. M. K. Airaksinen, A. O. I. Krause, J. Sainio, J. Lahtinen, K. J. Chao, M. O. G. Pérez, M. A. Bañares, *Phys. Chem. Chem. Phys.* **2003**, 5, 4371-4377.

[46] A. Hakuli, A. Kytökivi, A. O. I. Krause, T. Suntola, *Appl. Catal. A* **2000**, 190, 219-232.

[47] L. Liu, H. Li, Y. Zhang, *J. Phys. Chem. B* **2006**, 110, 15478-15485.

[48] A. Hakuli, A. Kytökivi, A. O. I. Krause, T. Suntola, *J. Catal.* **1996**, 161, 393-400.

[49] M. Lezanska, G. S. Szymanski, P. Pietrzyk, Z. Sojka, J. A. Lercher, *J. Phys. Chem. C* **2007**, 111, 1830-1839.

[50] M. S. Kumar, N. Hammer, M. Rønning, A. Holmen, D. Chen, J. C. Walmsley, G. Øye, *J. Catal.* **2009**, 261, 116-128.

[51] S. S. Kim, T. R. Pauly, T. J. Pinnavaia, *Chem. Commun.* **2000**, 835-836.

[52] X. Zhao, X. Wang, *J. Mol. Catal. A: Chem.* **2007**, 225-231.

[53] L. Zhang, Y. Zhao, H. Dai, H. He, C. T. Au, *Catal. Today* **2008**, 131, 42-54.

[54] Y. Wang, Y. Ohishi, T. Shishido, Q. Zhang, W. Yang, Q. Guo, H. Wan, K. Takehira, *J. Catal.* **2003**, 220, 347-357.

[55] B. M. Weckhuysen, I. E. Wachs, R. A. Schoonheydt, *Chem. Rev.* **1996**, 96, 3327-3349.

[56] W. Zhang, B. Glomski, T. R. Pauly, T. J. Pinnavaia, *Chem. Commun.* **1999**, 1803-1804.

[57] M. A. Vuurman, F. D. Hardcastle, I. E. Wachs, *J. Mol. Catal.* **1993**, 84, 193-205.

[58] A. B. Gaspar, J. L. F. Brito, L. C. Dieguez, *J. Mol. Catal. A* **2003**, 203, 251-266.

[59] W. Zhang, T. J. Pinnavaia, *Catal. Lett.* **1996**, 38, 261-265.

[60] F. Cavani, M. Koutyrev, F. Trifirò, A. Bartolini, D. Ghisletti, R. Iezzi, A. Santucci, G. D. Piero, *J. Catal.* **1996**, 158, 236-250.

[61] P. Michorczyk, J. Ogonowski, P. Kuśtrowski, L. Chmielarz, *Appl. Catal. A* **2008**, 349, 62-69.

[62] C. Li, P. C. Stairs, *Stud. Surf. Sci. Catal.* **1996**, 101, 881-890.

[63] P. McMillan, B. Piriou, *J. Non-cryst. Solids* **1982**, 53, 279-298.

[64] T. Ivanova, K. Gesheva, A. Cziraki, A. Szekeres, E. Vlaikova, *J. Phys.: Conf. Ser.* **2008**, 113, 012030.

[65] A. Hakuli, M. E. Harlin, L. B. Backman, A. O. I. Krause, *J. Catal.* **1999**, 184, 349-356.

[66] L. Liu, H. Li, Y. Zhang, *Catal. Today* **2006**, 115, 235-241.

[67] B. M. Weckhuysen, I. E. Wachs, *J. Phys. Chem.* **1996**, 100, 14437-14442.

[68] T. Shishido, K. Shimamura, K. Teramura, T. Tanaka, *Catal. Today* **2012**, 185, 151-156.

[69] B. M. Weckhuysen, R. A. Schoonheydt, *Catal. Today* **1999**, 51, 223-232.

[70] A. Bruckner, *Chem. Commun.* **2001**, 20, 2122-2123.

[71] A. Bruckner, *Phys. Chem. Chem. Phys.* **2003**, 5, 4461-4472.

[72] T. A. Nijhuis, S. J. Tinnemans, T. Visser, B. M. Weckhuysen, *Phys. Chem. Chem. Phys.* **2003**, 5, 4361-4365.

[73] T. A. Nijhuis, S. J. Tinnemans, T. Visser, B. M. Weckhuysen, *Chem. Eng. Sci.* **2004**, 59, 5487-5492.

[74] S. D. Rossi, G. Ferraris, S. Fremiotti, E. Garrone, G. Ghiotti, M. C. Campa, V. Indovina, *J. Catal*. **1994**, 148, 36-46.

[75] B. M. Weckhuysen, A. Bensalem, R. A. Schoonheydt, *J. Chem. Soc., Faraday Trans.* **1998**, 94, 2011-2014.

[76] R. L. Puurunen, B. M. Weckhuysen, *J. Catal.* **2002**, 210, 418-430.

[77] M. Chen, J. Xu, Y. M. Liu, Y. Cao, H. Y. He, J. H. Zhuang, *Appl. Catal. A* **2010**, 377, 35-41.

[78] P. Michorczyk, J. Ogonowski, *Appl. Catal. A* **2003**, 251, 425-433.

[79] P. Michorczyk, J. Ogonowski, *React. Kinet. Catal. Lett.* **2006**, 87, 177-183.

[80] M. M. Bettahar, G. Costentin, L. Savary, J.C. Lavalley, *Appl. Catal. A* **1996**, 145, 1-48.

[81] S. Wang, Z. H. Zhu, *Energ. Fuel*. **2004**, 18, 1126-1139.

[82] P. Michorczyk, K. Góra-Marek, J. Ogonowski, *Catal. Lett.* **2006**, 109, 195-198.

[83] T. Shishido, K. Shimamura, K. Teramura, T. Tanaka, *Catal. Today* **2012**, 185, 151-156.

[84] X. Zhang, Y. Yue, Z. Gao, *Catal. Lett.* **2002**, 83, 19-25.

[85] I. Takahara, W.-C. Chang, N. Mimura, M. Saito, *Catal. Today* **1998**, 45, 55-59.

[86] L.-Ch. Liu, H.-Q. Li, Y. Zhang, *Kinet. Catal.* **2009**, 50, 684-690.

[87] S. M. K. Airaksinen, A. O. I. Krause, J. Sainio, J. Lahtinen, K. Chao, M. O. Guerrero-Pérez, M. A. Bañares, *Phys. Chem. Chem. Phys.* **2003**, 5, 4371-4377.

[88] M. Lezanska, G. S. Szymanski, P. Pietrzyk, Z. Sojka, J. A. Lercher, *J. Phys. Chem. C* **2007**, 111, 1830-1839.

[89] A. Hakuli, A. Kytökivi, A. O. I. Krause, T. Suntola, *J. Catal.* **1996**. 161, 393-400.

[90] M. S. Kumar, N. Hammer, M. Rønning, A. Holmen, D. Chen, J. C. Walmsley, G. Øye, *J. Catal.* **2009**, 261, 116-128.

[91] A. Hakuli, M. E. Harlin, L. B. Backman, A. O. I. Krause, *J. Catal.* **1999**, 184, 349-356.

[92] A.B. Gaspar, J.L.F. Brito, L.C. Diequez, *J. Mol. Catal. A* **2003**, 203 251-266.

[93] K. Takehira, Y. Ohishi, T. Shishido, T. Kawabata, K. Takaki, Q. Zhang, Y. Wang, *J. Catal.* **2004**, 224, 404-416.

[94] K. Nakagawa, C. Kajita, N. Ikenaga, M. Nishitani-Gamo, T. Ando, T. Suzuki, *Catal. Today* **2003**, *84*, 149-157.

[95] S. N. Riduan, Y. Zhang, *Dalton Trans.* **2010**, 39, 3347-3357.

[96] M.A. Botavina, G. Martra, Y. A. Agafonov, N. A. Gaidai, N. V. Nekrasov, D.V. Trushin, S. Coluccia, A. L. Lapidus, *Appl. Catal. A* **2008**, 347, 126-132.

[97] A. E, C. Luna , M. E. Iriarte, *Appl. Catal. A* **2008**, 343, 10-15.

[98] S. He, Q. Jing, W. Yu, L. Mo, H. Lou, X. Zheng, *Catal. Today* **2009**, 148, 130-133.

[99] S. F. He, H. M. Wu, W. J. Yu, L. Y. Mo, H. Lou, X. M. Zheng, *Int. J. Hydrogen Energy* **2009**, 34, 839-843.

[100] W. Luhui, Z. Shaoxing, L. Yuan, *J. Rare. Earth.* **2008**, 26, 66-70.

[101] A. M. Mebel, D.Y. Hwang, *J. Phys. Chem. A* **2000**, 104, 11622-11627.

[102] S. J. Choe, H. J. Kang, D. H. Park, D. S. Huh, J. Park, *Appl. Surf. Sci.* **2001**, *181*, 265-276.

[103] F. Cavani, M. Koutyrev, F. Trifiró, A. Bartolini, D. Ghisletti, R. Iezzi, A. Santucci, G. D. Piero, *J. Catal.***1996**, 158, 236-250.

[104] L. Zhang, Y. Zhao, H. Dai, H. He, C.T. Au, *Catal. Today* **2008**, 131, 42-54.

[105] L. Chmielarz, P. Kuśtrowski, M. Kruszec, R. Dziembaj, *J. Porous. Mat.* **2005**, 12, 183-191.

[106] T. P. Maniecki, *Catal. Today* **2011**, 176, 215-218.

[107] S. S. A. Syed-Hassan, C. Z. Li, *Appl. Catal. A* **2011**, 398, 187-194.

[108] L.B. Råberg, M.B. Jensena, U. Olsbye, C. Daniel, S. Haag, C. Mirodatos, A. O. Sjåstad, *J. Catal.* **2007**, 249, 250-260.

[109] S. J. Choe, H. J. Kang, S.J. Kim, S.B. Park, D. H. Park, D. S. Huh, *Bull. Korean Chem. Soc.* **2005**, 26, 1682-1688.

[110] B. M. Weckhuysen, I. E. Wachs, *J. Phys. Chem.* **1996**, 100, 14437-14442.

[111] J. B. Wang, L.E. Kuo, T.J. Huang, *Appl. Catal. A* **2003**, 249, 93-105.

[112] B. Mile, D. Stirling, M. A. Zammitt, A. Lovell, *J. Catal.* **1988**, 114, 217-229.

[113] B. M. Weckhuysen, I. E. Wachs, R. A. Schoonheydt, *Chem. Rev.* **1996**, 96, 3327-3349.

[114] D. Stoiljkovi ć , B. Pili ć, M. Bulaji ć, N. Đurasovi ć, N. Ostrovski, *J. Serb. Chem. Soc.* **2007**, 72(11), 1155-1169.

[115] E. Groppo, C. Lamberti, G. Spoto, S. Borkiga, G. Magnacca, A. Zecchina, *J. Catal.* **2005**, 236, 233-244.

[116] P. Michorczyk, J. Ogonowski, *React. Kinet. Catal. Lett.* **2007**, 92, 61-68.

[117] Y. Ohishi, T. Kawabata, T. Shishido, K. Takaki, Q. Zhang, Y. Wang, K. Takehira, *J. Mol. Catal. A* **2005**, *230*, 49-58.

[118] A. Cimino, B. A. D. Angelis, A. Luchetti, G. Minelli, *J. Catal.* **1976**, 45, 316-325.

[119] R. Merryfield, M. Mcdaniel, G. Parks, *J. Catal.* **1982**, 77, 348-359.

[120] T. V. M. Rao, E. M. Zahidi, A. Sayari, *J. Mol. Catal. A* **2009**, 301, 159-165.

[121] D. Zhao, J. Sun, Q. Li, G. D. Stucky, *Chem. Mater.* **2000**, 12, 275-279.

[122] a) J. R. Regalbuto, *Science* **2009**, 325, 822-824; b) G. M. Whitesides, G. W. Crabtree, *Science* **2007**, 315, 796-798; c) F. W. Lichtenthaler, S. Peters, *C. R. Chim.* **2004**, 7, 65-90; d) J. N. Chheda, G. W. Huber, J. A. Dumesic, *Angew. Chem.* **2007**, 119, 7298-7318; *Angew. Chem. Int. Ed.* **2007**, 46, 7164-7183; e) A. Corma, S. Iborra, A. Velty, *Chem. Rev.* **2007**, 107, 2411-2502; f) P. Gallezot, *ChemSusChem* **2008**, 1, 734-737.

[123] a) C. Y. Ng, M. Y. Jung, J. Lee, M. K. Oh, *Microb. Cell Fact.* **2012**, 11, 68; b) M. –J. Syu, *Appl. Microbiol. Biotechnol.* **2001**, 55, 10-18; c) J. G. Zeikus, M. K. Jain, P. Elankovan, *Microb. Cell Fact.* **1999**, 51, 545-552.

[124] a) L. Johansen, K. Bryn, F. C. Størmer, *J. Bacteriol.* **1975**, 123, 1124-1130; b) A. Orjuela, A. Kolah, C. T. Lira, D. J. Miller, *Ind. Eng. Chem. Res.* **2011**, **50**, 9209-9220.

[125] a) X. J. Ji, H. Huang, J. Du, J. G. Zhu, L. J. Ren, S. Li, Z. K. Nie, *Bioresour. Technol.* **2009**, 100, 5214-5218; b) L. Ge, X. Wu, J. Chen, J. Wu, *J. Biomater. Nanobiotechnol.* **2011**, 2, 335-336; c) M. Anvari, M. R. S. Motlagh, *J. Biomed. Biotechnol.* **2010**, 2011; d) M. Anvari, G. Khayati, *Asian J. Chem.* **2009**, 21, 2131-2140; e) S. H. Shin, S. Kim, J. Y. Kim, S. Lee, Y. Um, M. K. Oh, Y. R. Kim, J. Lee, K. S. Yang, *J. Bacteriol*. **2012**, 194, 2736-2737. The high price of 1,3-butadiene can be obtained from Duncan Seddon & Associates Pty. Ltd. via http://www.duncanseddon.com/docs/pdf/the-high-price-of-butadiene.pdf.

[126] a) N. L. Morrow, *Environ. Health Perspect.* **1990**, 86, 7-8; b) A. Singh, A. Chavda, S. Nandula, R. V. Jasra, M, Maiti, *Ind. Eng. Chem. Res.* **2012**, 51, 11066-11071; c) European Commission. **2007**. European Union Risk Assessment Report. 1,3-butadiene. CAS No: 106-66-0. EINECS No: 203-450-8. This report can be obtained free of charge via http://echa.europa.eu/documents/10162/1f512549-5bf8-49a8-ba51-1cf67dc07b72.

[127] W. C. White, *Chem. Biol. Interact.* **2007**, 166, 10-14.

[128] a) N. Shlechter, D. F. Othmer, S. Marshak, *Ind. Eng. Chem.* **1945**, 37, 900-905; b) N. Shlechter, D. F. Othmer, R. Brand, *Ind. Eng. Chem.* **1945**, 37, 905-908.

[129] A. J. L. Jesus, M. T. S. Rosado, I. Reva, R. Fausto, M. E. Euse´bio, J. S. Redinha, *J. Phys. Chem. A* **2006**, 110, 4169-4179.

[130] a) K. M. Parida, S. Mallick, *J. Mol. Catal. A: Chem.* **2007**, 275, 77-83; b) K. Saravanan, B. Tyagi, H. C. Bajaj, *Catal. Sci. Technol.* **2012**, 2, 2512-2520;

c) K. Mantri, K. Komura, Y. Sugi, *Green Chem.* **2005**, 7, 677-682; d) S.S. Dash, K.M. Parida, *J. Mol. Catal. A: Chem.* **2007**, 266, 88-92.

[131] a) W. Zhang, D. Yu, X. Jia, H. Huang, *Green Chem.* **2012**, 14, 3441; b) A. V. Tran, R. P. Chambers, *Biotechnol. Bioeng.* **1987**, 29, 343-351.

[132] W. H. Brown, C. S. Foote, B. L. Iverson, *Organic Chemistry*, Brooks/Cole Publishing Inc., California, 4th edn, **2005**.

[133] Y. Miyano, K. Fukuchi, *Fluid. Phase. Equilib*. **2004**, 226, 183-187.

[134] J. Yu, P. E. Savage, *Ind. Eng. Chem. Res*. **1998**, 37, 2-10.

[135] A. N. Bourns, R. V. V. Nicholls, *Can. J. Res.* **1947**, 25b, 80-89.

[136] J. M. Park, H. Song, H. J. Lee, D. Seung, Microb. Cell Fact. **2013**, 12, 20-31.

# 국 문 초 록

올레핀(Olefin)과 다이올레핀(Diolefin)은 탄소 이중결합이 한 개 이상 존재하는 화합물을 지칭하며 에틸렌(Ethylene), 프로필렌(Propylene), 부틸렌(Butylene)이 그에 해당한다. 이러한 화합물은 화학 산업에서 기초 단위의 물질로 주로 사용되며 세계적으로 가장 많은 생산 비율을 차지하고 있을 만큼 매우 중요한 화합물이다. 올레핀과 다이올레핀은 일반적으로 나프타(Naphtha)의 수증기 분해(Steam cracking)로 얻어지는데 석유 고갈 문제와 더불어, 이러한 화합물을 얻을 수 있는 새로운 자원을 개발하는 것이 중요하다. 가장 대표적인 대체 자원으로는 석탄(Coal), 천연가스(Natural gas), 바이오매스(Biomass)를 들 수 있다. 위와 같은 대체 자원으로부터 올레핀과 다이올레핀을 효율적으로 얻기 위한 연구가 수 년간 많이 진행되어 왔으며, 촉매 연구 분야에서 가장 주목 받고 있는 연구 중 하나이다. 이 학위논문은 대체 자원 중의 하나인 천연가스와 바이오매스를 기반으로 하여 프로필렌과 1,3-부타디엔(1,3-Butadiene)을 효율적으로 생산하기 위한 촉매 및 반응 개발에 대하여 다루고 있다. 자세한 내용은 다음과 같다.

크롬 산화물(Chromium oxide)은 이산화탄소를 사용한 프로판(Propane)의 탈수소화 반응(Dehydrogenation)에 뛰어난 활성을 가진

물질로 알려져 있다. 하지만, 벌크(Bulk) 크롬 산화물은 낮은 표면적으로 인하여 쉽게 활성을 잃어버리는 단점을 지닌다. 따라서, 활성점을 최대한 많이 활용 및 유지하기 위하여 중형기공 실리카에 고분산 된 크롬 산화물을 솔-젤(Sol-gel) 방법으로 제조하였다. 승온 환원법 (Temperature-programmed reduction)을 통하여 단량체의 크롬 6가 (Isolated Cr (VI))와 이량체 이상의 크롬 6가(Polymeric Cr (VI)) 두 가지 형태의 크롬 산화물이 존재한다는 것을 알아내었고 이량체 이상의 크롬 6가가 많이 존재할수록 이산화탄소를 사용한 프로판의 탈수소화 반응에 효과적이라는 것을 알 수 있었다.

크롬 산화물은 이산화탄소를 사용한 프로판의 탈수소화 반응에서 다음과 같은 두 가지 요인으로 인하여 비활성화 현상을 보인다. 첫 번째는 코크(Coke) 침적에 의한 접촉 가능한 촉매 활성점의 손실이며 두 번째는 크롬의 환원으로 인한 활성점의 변화를 들 수 있다. 이번 연구를 통하여 두 가지 비활성화 원인 중 크롬의 환원이 주 원인으로 밝혀졌고 환원된 크롬을 재생시키고자 니켈(Ni)을 조촉매로 사용하였다. 니켈은 이산화탄소를 분해하여 일산화탄소와 활성화된 산소를 생성한다. 활성화된 산소는 환원된 크롬을 다시 산화시켜 장시간 동안 이산화탄소를 사용한 프로판의 탈수소화 반응에서 활성을 보이는 안정한 촉매를 제조할 수 있었다.

마지막으로, 글루코오스 발효액으로부터 유래한 2,3-부탄디올을

이용하여 1,3-부타디엔을 생산하는 새로운 공정을 두 가지 접근법을 통하여 개발하였다. 먼저, 2,3-부탄디올과 더불어 글루코오스 발효액의 부산물인 개미산(Formic acid)과 아세트산(Acetic acid)을 이용하여 에스터화 반응(Esterification)과 열분해반응(Pyrolysis)을 거쳐 1,3-부타디엔을 생산할 수 있는 공정을 개발하였다. 또한, 탈수화 반응(Dehydration)과 이성질화 반응(Isomerization)이 결합된 비균일 촉매 반응을 통하여 1,3-부타디엔을 높은 수율로 얻을 수 있었다. 이러한 새로운 촉매 공정 연구를 통하여 석유기반 공정을 대체할 수 있는 환경친화적 공정을 개발할 수 있었다.

**주요어:** 크롬 산화물, 프로필렌, 이산화탄소를 이용한 프로판의 탈수소화 반응, 니켈 조촉매, 글루코오스 발효액, 에스테르화 반응과 열분해 반응, 1,3-부타디엔
**학 번:** 2009-20997

# List of publications

## International Publications

## International Academic Published Papers (First Author)

1. T. Y. Kim*, **J. Baek***, C. K. Song, Y. S. Yun, D. S. Park, W. Kim, J. W. Han, and J. Yi, "Gas-phase Dehydration of Vicinal Diols to Epoxides: Dehydrative Epoxidation over a $Cs/SiO_2$ catalyst", Journal of Catalysis, 323, 85-99 (2015)
   (* Jayeon Baek and Tae Yong Kim contributed equally to this work.)
2. **J. Baek***, T. Y. Kim*, W. Kim, H. J. Lee, and J. Yi, "Selective Production of 1,3-Butadiene using Glucose Fermentation Liquor", Green Chemistry, 16(7), 3501-3507 (2014)
   (* Jayeon Baek and Tae Yong Kim contributed equally to this work.)
3. M. Eo*, **J. Baek***, H. D. Song, S. Lee, and J. Yi, "Quantification of Electron Transfer Rates of Different Facets on Single Gold Nanoparticles During Catalytic Reaction", Chemical Communications, 49(45), 5204-5206 (2013)
   (* Jayeon Baek and Moonjung Eo contributed equally to this work)
4. D. Yun*, **J. Baek***, Y. Choi, W. Kim, H. J. Lee, and J. Yi, "Promotional Effect of Ni on a $CrO_x$ Catalyst Supported on Silica in the Oxidative Dehydrogenation of Propane using $CO_2$", ChemCatChem, 4(12), 1952-1959 (2012).
   (* Jayeon Baek and Danim Yun contributed equally to this work)
5. **J. Baek**, H. J. Yun, D. Yun, Y. Choi, and J. Yi, "Preparation of Highly Dispersed Chromium Oxide Catalysts Supported on Mesoporous Silica for the Oxidative Dehydrogenation of Propane using $CO_2$: Insight into the Nature of Catalytically Active Chromium Sites", ACS Catalysis, 2(9), 1893-1903 (2012)

## International Academic Published Papers (Co-author)

1. D. S. Park*, D. Yun*, T. Y. Kim, **J. Baek**, Y. S. Yun, and J. Yi, "A Mesoporous Carbon-Supported Pt Nanocatalyst for the Conversion of Lignocellulose to Sugar Alcohols", ChemSusChem, 6(12), 2281-2289 (2013)
   (* Dae Sung Park and Danim Yun contributed equally to this work.)
2. Y. Choi, D. S. Park, H. J. Yun, **J. Baek**, D. Yun, and J. Yi, "Mesoporous Siliconiobium Phosphate as a Pure Brønsted Acidic Catalyst with Excellent Performance for the Dehydration of Glycerol to Acrolein", ChemSusChem, 5(12), 2460-2468 (2012)
3. T. Y. Kim, D. S. Park, Y. Choi, **J. Baek**, J. R. Park, and J. Yi, "Preparation and Characterization of Mesoporous Zr-$WO_x/SiO_2$ Catalysts for the Esterification of 1-Butanol with Acetic Acid", Journal of Materials Chemistry, 22(19), 10021-10028 (2012)
4. Y. Choi, N. D. Kim, **J. Baek**, W. Kim, H. J. Lee, and J. Yi, "Effect of $N_2O$-Mediated Calcination on Nickel Species and the Catalytic Activity of Nickel Catalysts Supported on $\gamma$-$Al_2O_3$ in the Steam Reforming of Glycerol", International Journal of Hydrogen Energy, 36(6), 3844-3852 (2011)

## Domestic Publications (Korean journal)

1. **백자연**, 윤형진, 김남동, 최영보, 이종협, "Keggin형 헤테로폴리산에 의한 과당의 5-하이드록시메틸퍼퓨랄로의 전환을 위한 탈수반응", Clean Technology, 16(3), 220-228 (2010)

## Patents Application on File

1. 이종협, 김태용, 박대성, 최영보, **백자연**, 박재률, "균일한 중형 기공을 갖는 복합 산화물 촉매, 그 제조 방법 및 상기 촉매를 이용하여 에스테르 화합물을 제조하는 방법", 특허 출원 10-2012-0053823 (2012.05.21)

2. 이종협, 최영보, **백자연**, 김우영, 이희종, "중형 기공성 니오븀- 실리케이트- 포스페이트 복합체, 그 제조방법 및 이를 이용하여 2,3-부탄디올로부터 메틸에틸케톤을 제조하는 방법", 특허 출원 10-2011-0000840 (2011.01.05)
3. 이종협, **백자연**, 최영보, 김우영, 이희종, 차규섭, "크롬 산화물이 분산된 알루미나 촉매, 이의 제조방법 및 이를 이용하여 프로필렌을 제조하는 방법", 특허 출원 10-2010-0140062 (2010.12.31)

## International Conferences (First author)

1. **J. Baek**, S. K. Song, T. Y. Kim, K. R. Lee, H. Park, D. Yun, and J. Yi, "Facile Preparation and Characterization of 3D Flower-like Rutile Titania and Its Application to the Plasmonic Photocatalysis", MRS Fall Meeting Program & Exhibit, Boston, MA, USA, November 30-December 5 (2014)
2. **J. Baek**, T. Y. Kim, I. Nam, S. Park, S. Yu, S. Bae, S. Y. Lee, H. N. Umh, Y. H. Kim, and J. Yi, "Production of Valuable Chemicals (1,3-Butadiene) from Biomass-Based Resources Alternative to the Petroleum", 248$^{th}$ ACS National Meeting & Exposition, San Francisco, CA, USA, August 10-14 (2014)
3. **J. Baek**, T. Y. Kim, W. Kim, W. K. Synn, H. J. Lee, and J. Yi, "New Synthetic Pathway for the Catalytic Production of 1,3-Butadiene Using 2,3-Butanediol and Succinic Acid Derived from Glucosic Biomass", The 14$^{th}$ Japan-Korea Symposium on Catalysis, WINC Aichi, Nagoya, Japan, July 1-3 (2013)
4. **J. Baek**, M. Eo, H. D. Song, S. Lee, and J. Yi, "Quantified Electron Transfer Rate on Single Gold Nanoparticles with Different Facets During Catalytic Reaction", The 6$^{th}$ WCU International Symposium on Chemical Convergence for Energy and Environment, Sheraton Hotel, Incheon, Korea, June 17-18 (2013)
5. **J. Baek**, N. D. Kim, Y. Choi, and J. Yi, "Preparation and Characterization of Mesoporous Ceria-Based Catalysts for the Production of Propylene from $CO_2$ and Propane", 240$^{th}$ ACS National Meeting and Exposition, Boston, MA, USA, August 22-26 (2010)

## International Conferences (Co-author)

1. D. S. Park, D. Yun, Y. S. Yun, H. Park, T. Y. Kim, **J. Baek**, and J. Yi, "Direct Conversion of Lignocellulose to Sugar Alcohols over Pt Supported on a New 3D Mesoporous Carbon", 247th ACS National Meeting & Exposition, Dallas, Texas, USA, March 16-20 (2014)
2. T. Y. Kim, **J. Baek**, W. Kim, W. K. Synn, H. J. Lee, and J. Yi, "Novel Catalytic Routes for the Selective Production of 1,3-Butadiene from Biomass Derived 2,3-Butanediol", The 14th Japan-Korea Symposium on Catalysis, WINC Aichi, Nagoya, Japan, July 1-3 (2013)
3. T. Y. Kim, S. Yu, **J. Baek**, and J. Yi, "Effect of Zr/W Ratio on Mesoporous Zr-$WO_x/SiO_2$ as a Solid Acid: Formation and Optimization of Zr-$WO_x$ Clusters", 244th ACS National Meeting & Exposition, Philadelphia, Pennsylvania, USA, August 19-23 (2012)
4. H. J. Yun, H. Lee, N. D. Kim, M. Lee, S. Yu, **J. Baek**, Y. Choi and J. Yi, "Facile Adjustment of Doping Level in Carbon Doped $TiO_2$ Nanoparticle", 218th ECS Meeting, Las Vegas, Nevada, USA, October 10-15 (2010)
5. Y. Choi, N. D. Kim, **J. Baek**, and J. Yi, "Preparation and Characterization of Highly Active Ni Catalyst Supported on $\gamma$-$Al_2O_3$ for the Steam Reforming of Glycerol", 240th ACS National Meeting and Exposition, Boston, MA, USA, August 22-26 (2010)

## Domestic Conferences

1. 송찬경, **백자연**, 김태용, 유성주, 이종협, "계층 구조를 가진 3차원 TiO2의 제조 및 이를 이용한 페놀 광분해 반응에의 응용", 추계한국청정기술학회, 경주 K호텔, 9 .24-26 (2014)
2. 김태용, **백자연**, 송찬경, 윤양식, 박대성, 이종협, "밀도범함수이론을 이용한 바이오매스 유래 2,3-부탄디올의 2,3-에폭시부탄으로의 전환에 대한 연구", 추계한국청정기술학회, 경주 K호텔, 9. 24-26 (2014)

3. **백자연**, 김태용, 박대성, 박홍석, 송찬경, 이경록, 이종협, “글루코오스 발효액으로부터의 1,3-부타디엔 생성”, 춘계한국화학공학회, 창원컨벤션센터, 4. 23-25 (2014)
4. 윤양식, 박홍석, 윤다님, 박대성, 김태용, **백자연**, 이경록, 이종협, “계층구조를 갖는 나노크기의 고체산촉매 제조 및 응용”, 춘계한국청정기술학회, 여수경도리조트, 3. 27-28 (2014)
5. **백자연**, 김태용, 송찬경, 이종협, “글루코오스 발효액을 이용한 1,3-부타디엔 생성 반응”, 춘계한국청정기술학회, 여수경도리조트, 3. 27-28 (2014)
6. 김태용, **백자연**, 송찬경, 윤양식, 박대성, 한정우, 이종협, “바이오매스 유래물질의 맞춤형 탈수반응을 위한 비시널 디올로부터 에폭사이드 유래물질 생성”, 춘계한국청정기술학회, 여수경도리조트, 3. 27-28 (2014)
7. **백자연**, 송현돈, 김태용, 박대성, 윤다님, 윤양식, 박홍석, 이종협, “금 나노입자의 암모니아 보란을 이용한 4-니트로페놀 환원 반응에서의 실시간 전자이동 관찰”, 추계한국청정기술학회, 제주한화리조트, 9. 25-27 (2013)
8. 김태용, **백자연**, 김우영, 신우균, 이희종, 이종협, “고부가가치 1,3-부타디엔의 생산을 위한 바이오매스 유래 2,3-부탄디올의 전환 및 이를 위한 촉매 공정”, 춘계한국청정기술학회, 여수경도리조트, 3. 28-29 (2013)
9. **백자연**, 윤다님, 최영보, 김태용, 김우영, 이희종, 김영훈, 이종협, “이산화탄소/프로판을 원료로 사용하는 프로필렌 제조용 촉매 공정 개발 1. 고효율 촉매 설계 및 제조”, 추계한국청정기술학회, 영남대학교, 11. 16 (2012)
10. 김태용, 박대성, **백자연**, 최영보, 김영훈, 이종협, “바이오매스 유래 알코올과 유기산의 고부가가치용 촉매개발 연구”, 추계한국청정기술학회, 영남대학교, 11. 16 (2012)
11. 윤다님, **백자연**, 최영보, 김우영, 이희종, 김영훈, 이종협, “이산화탄소/프로판을 원료로 사용하는 프로필렌 제조용 촉매 공정 개발 2. 안정성 최대화 촉매 개발”, 추계한국청정기술학회, 영남대학교, 11. 16 (2012)
12. 최영보, 박대성, **백자연**, 윤다님, 이종협, “바이오매스 유래 글리세롤의 고부가가치용 촉매 개발 1. 고효율 촉매 설계 및 제조”, 추계한국청정기술학회, 영남대학교, 11. 16 (2012)
13. 윤다님, **백자연**, 최영보, 김우영, 이희종, 이종협, “이산화탄소와 프로판으

로부터 프로펄렌 제조를 위한 $CrO_x$/SBA-15 촉매의 니켈 첨가에 의한 영향", 추계한국화학공학회, 부산BEXCO, 10. 24-26 (2012)

14. 어문정, **백자연**, 이수승, 송현돈, 이종협, "단일 금 나노입자 촉매상에서의 4-니트로페놀 환원 반응 실시간 관찰", 추계한국화학공학회, 부산BEXCO, 10. 24-26 (2012)
15. **백자연**, 윤다님, 윤형진, 최영보, 김우영, 이희종, 이종협, "중형기공실리카에 크롬산화물이 고분산된 Cr-MSU-x 촉매의 제조 및 이산화탄소를 산화제로 사용한 프로판의 산화 탈수소화 반응(ODHP)에서의 촉매특성연구", 추계한국화학공학회, 부산BEXCO, 10. 24-26 (2012)
16. 김태용, 박대성, 최영보, **백자연**, 이종협, "바이오매스로부터 고부가가치 화학물질 제조와 중형기공성 Zr-$WO_x$/$SiO_2$ 촉매의 개발", 춘계한국청정기술학회, 연세대학교, 5.25 (2012)
17. 김태용, 박대성, 최영보, **백자연**, 박재률, 이종협, "부탄올 에스테르화 반응을 위한 중형기공의 Zr-$WO_x$/$SiO_2$ 촉매의 제조 및 특성 분석", 춘계한국화학공학회, 제주국제컨벤션센터, 4.25-27 (2012)
18. **백자연**, 윤다님, 윤형진, 최영보, 김우영, 이희종, 이종협, "이산화탄소를 산화제로 사용한 프로판의 산화 탈수소화 반응(ODHP)에서의 Cr-MSU-x 촉매 특성연구", 추계한국화학공학회, 송도컨벤시아, 10. 26-28 (2011)
19. 최영보, 박대성, 윤형진, **백자연**, 윤다님, 이종협, "새로운 산촉매 개발과 글리세롤 탈수 반응에의 적용", 추계한국화학공학회, 송도컨벤시아, 10. 26-28 (2011)
20. 윤형진, 이민재, 유성주, **백자연**, 최영보, 이종협, "다양한 형태의 $TiO_2$ 나노입자 제조 및 광촉매 특성 변화", 추계한국청정기술학회, 충남대학교, 11. 19 (2010)
21. **백자연**, 윤형진, 김남동, 최영보, 이종협, "헤테로폴리산 $H_nXM_{12}O_{40}$ (중심원소 X = P, Si, 배위원소 M = W, Mo)을 이용한 과당으로부터 5-Hydroxymethylfurfural의 탈수화 반응 연구", 추계한국화학공학회, 대전컨벤션센터, 10. 20-22 (2010)
22. 최영보, 김남동, **백자연**, 김우영, 이희종, 이종협, "글리세롤의 수증기 개질반응: 일산화이질소 분위기에서 소성한 니켈 담지 촉매의 활성과 열역학

적 평형 조성의 비교", 추계한국화학공학회, 대전컨벤션센터, 10. 20-22 (2010)

23. 곽병규, 김남동, 박대성, **백자연**, 최영보, 박재률, 김우영, 이종협, "Organosilicate를 이용한 균일한 크기의 중형기공 탄소체의 합성", 춘계화학공학회, 대구EXCO, 4. 21-23 (2010)
24. **백자연**, 오석일, 최영보, 정광섭, 이종협, "Synthesis of 5-Hydroxymethyl-Fufural (HMF) from Fructose Using Heteropolyacid Catalysts Supported on Inorganic Supports", 추계화학공학회, 일산KINTEX, 10.21-23 (2009)